2008

Energetic and Entropic Elasticity of Nonisothermal Flowing Polymers: Experiment, Theory, and Simulation

David J. Keffer
University of Tennessee - Knoxville

T. C. Ionescu
University of Tennessee - Knoxville

B. J. Edwards
University of Tennessee - Knoxville

V. G. Mavrantzas
University of Patras

Recommended Citation

Energetic and entropic elasticity of nonisothermal flowing polymers: Experiment, theory, and simulation T. C. Ionescu, B. J. Edwards, D. J. Keffer, and V. G. Mavrantzas, J. Rheol. 52, 105 (2008), DOI:10.1122/1.2798235

Energetic and entropic elasticity of nonisothermal flowing polymers: Experiment, theory, and simulation

T. C. Ionescu, B. J. Edwards,[a)] and D. J. Keffer

Department of Chemical Engineering, University of Tennessee, Knoxville, Tennessee 37996

V. G. Mavrantzas

Department of Chemical Engineering, University of Patras and FORTH-ICE/HT, Patras, Greece, GR 26504

(Received 29 November 2006; final revision received 1 June 2007)

Synopsis

The thermodynamical aspects of polymeric liquids subjected to nonisothermal flow are examined from the complementary perspectives of theory, experiment, and simulation. In particular, attention is paid to the energetic effects, in addition to the entropic ones, that occur under conditions of extreme deformation. Comparisons of experimental measurements of the temperature rise generated under elongational flow at high strain rates with macroscopic finite element simulations offer clear evidence of the persistence and importance of energetic effects under severe deformation. The performance of various forms of the temperature equation are evaluated with regard to experiment, and it is concluded that the standard form of this evolution equation, arising from the concept of purely entropic elasticity, is inadequate for describing nonisothermal flow processes of polymeric liquids under high deformation. Complete temperature equations, in the sense that they possess a direct and explicit dependence on the energetics of the microstructure of the material, provide excellent agreement with experimental data. © *2008 The Society of Rheology.* [DOI: 10.1122/1.2798235]

I. INTRODUCTION

In the late 1990s, Dressler *et al.* (1999) published a short review of theoretical aspects of nonisothermal polymer flow research over the previous five or six decades. At the time that article was published, one of the prime conclusions was that not much work had been done on the subject relative to its enormous importance in the plastics processing industry. However, the article of Dressler *et al.*, as well as an almost simultaneous article by Wapperom and Hulsen (1998), laid a foundation for more progress in the current century by deriving complete forms of the temperature equation for materials with internal microstructure.

As described in the preceding article, progress in the theoretical aspects of nonisothermal polymer flows has possibly been hindered over the past three decades by the adoption of the theory of purely entropic elasticity, which was far from proven when it was

[a)]Author to whom correspondence should be addressed; electronic mail: bje@utk.edu

first introduced in the mid-1970s. At that time, it was necessary for further progress in the area of nonisothermal rheology to limit the evolution equations of the system to the bare minimum for the sake of quantitative analysis. This intuitively reasonable assumption thus allowed for further progression of the subject. This theory came to dominate the collective thought processes concerning nonisothermal flows, and this situation remains well established even today. The primary manifestation of this incomplete theory is an evolution equation for the temperature field that is devoid of any direct microstructural information.

As mentioned above, the previously cited articles opened up new possibilities for the theoretical description of nonisothermal flows by deriving complete forms of the temperature equation, which did not inherently assume the veracity of the concept of purely entropic elasticity. These temperature equations fully accounted for the inherent microstructure of polymeric liquids. However, since publication of those articles, the research in this area has languished somewhat, never fully taking off in this new direction. In this article, the challenge is taken up again, this time by combining theoretical analysis with solid experimentation and simulation of nonisothermal flow processes of polymeric liquids.

II. THEORETICAL BACKGROUND

A. General equations

In a typical engineering analysis of an incompressible, isothermal polymeric flow, one has to solve a coupled set of evolution equations composed of the conservation of momentum and an appropriate constitutive relationship that relates the stress tensor field to the strain rate tensor. For example, in the case of the Upper-Convected Maxwell Model (UCMM), one has the equation set

$$\rho\frac{D\mathbf{v}}{Dt} = -\nabla p + \nabla\cdot\tau, \tag{1}$$

$$\overset{\nabla}{\tau} + \frac{1}{\lambda}\tau = G(\nabla\mathbf{v} + (\nabla\mathbf{v})^T), \tag{2}$$

where $\mathbf{v}$ is the velocity vector field, ρ is the fluid mass density, p is the hydrostatic pressure, τ is the extra stress tensor field, G is the elastic modulus, and λ is the relaxation time. The operator $D\cdot/Dt$ represents the substantial or material time derivative [Bird *et al.* (2002)]. The superimposed reverse hat denotes Oldroyd's contravariant deformational derivative [Oldroyd (1950)]. For isothermal flow problems, this equation set can be solved under appropriate initial and boundary conditions, subject to the incompressibility constraint of the divergence-free condition

$$\nabla\cdot\mathbf{v} = 0. \tag{3}$$

In the nonisothermal flow case, one has to add the energy conservation equation

$$\rho\frac{D\hat{U}}{Dt} = -\nabla\cdot\mathbf{q} - p\,\nabla\cdot\mathbf{v} + \tau:\nabla\mathbf{v} \tag{4}$$

to the above set of equations. In this expression, $\hat{U}$ is the internal energy per unit mass and $\mathbf{q}$ is the heat flux vector field. Furthermore, it is important to note that the UCMM constitutive equation, Eq. (2), has additional terms under nonisothermal conditions [Mar-

rucci (1972); Bird (1979); Wiest (1988); Wapperom and Hulen (1998); Dressler *et al.* (1999)].

B. Polymeric materials with purely entropic elasticity

In Eq. (4), the internal energy on the left side is not a quantity that can be measured directly, and a simplification needs to be made. In thermodynamics, the Helmholtz free energy is defined as the Legendre transform of the internal energy

$$A \equiv U - TS. \tag{5}$$

Astarita and Sarti (1976a) defined the "rate of accumulation of elastic energy," $\dot{E}$, as,

$$\dot{E} \equiv \dot{A} + S\dot{T}, \tag{6}$$

which, in view of Eq. (5), can be expressed as

$$\dot{E} = \dot{U} - T\dot{S}. \tag{7}$$

In Eqs. (6) and (7), the superimposed dot represents the substantial time derivative. For an isothermal process, the rate of accumulation $\dot{E}$ is identified with the rate of accumulation of Helmholtz free energy, $\dot{A}$.

It is instructive to consider both extremes of the rheological spectrum. When structureless, isotropic fluids are subjected to deformation, their configurational entropy does not change upon cessation of deformation, providing the flow is incompressible [Treloar (1975)]. In other words, the internal structure of a particular volume element is essentially the same whether or not the deformation is present. Therefore, it would be safe to assume that simple isotropic fluids can accumulate elastic energy only by compression, thus by an increase in internal energy,

$$\dot{E} = \dot{U}. \tag{8}$$

Rubbery solids lie on the opposite end of the spectrum. Under the doctrine of the very successful *Theory of Rubber Elasticity* (TRE) [Treloar (1975)], the materials presently under consideration are assumed to accumulate elastic energy primarily through a decrease in conformational entropy

$$\dot{E} = -T\dot{S}. \tag{9}$$

This significant decrease in entropy is associated with the lower number of available configurations of the extended chains.

Polymeric melts, which are *viscoelastic* in nature, lie somewhere between isotropic fluids and rubbery solids on the rheological spectrum. Recent advances in atomic force microscopy have made it possible to measure the mechanical properties of polymers at the molecular level. Consequently, a considerable amount of effort has been dedicated to measuring the elastic responses of single polymer chains in various media [Ortiz and Hadziioannou (1999); Lu *et al.* (2004); Nakajima *et al.* (2006); Shi *et al.* (2006)]. The general consensus is that when single polymer chains are extended, their elastic response can entirely be attributed to a decrease in configurational entropy. A recent molecular simulation study appeared to substantiate this idea [Bedrov and Smith (2003); Smith *et al.* (2005)]. In this study, the authors measured the elastic response of a single chain placed in a simulation box, which was then filled with a solvent (either chemically different or similar to the single chain). The authors then proceeded to extend the chain and map out its free energy using the "umbrella sampling" technique, while keeping the

surrounding solvent at equilibrium. They concluded that unless the chain reaches its length of maximum extension, the internal energy of the *system* does not change. By definition, the chain adopts its maximum extension when all the torsional angles are in the *trans* conformation, while the bond angles and bond lengths are at their equilibrium values. Clearly, the internal energy increase observed at the highest extensions was due to modifications in bond angles.

Our recent molecular simulation results [Ionescu *et al.* (2007)] suggest that when a polymer melt (or an ensemble of chains) is stretched, the most important contributor to the change in internal energy is the intermolecular nonbonded energy. The two other major contributors are the torsional energy and the intramolecular nonbonded energy, which are of about the same magnitude and opposite in sign, thereby canceling each other. Consequently, the results obtained by single-chain elasticity measurements are not at all surprising, since the medium surrounding the extended polymer chain was kept at equilibrium; thus the change in the nonbonded intermolecular energy was negligible. In reality, when a polymeric liquid experiences deformation, the macromolecular chains tend to align relative to the direction of the deformation, establishing more favorable side-side interactions with the neighboring chains. This plays a major role in the energy balance of the system, because these favorable interactions lower the intermolecular nonbonded energy significantly. In extreme cases, the oriented melts experience the phenomenon called "flow-induced crystallization." Indeed, we have shown evidence of crystalline-like structures forming during simulation of *n*-eicosane subjected to planar elongational flow [Ionescu *et al.* (2006)].

If we examine the internal structure of cross-linked rubbery solids, the chain segments connecting two network nodes can be modeled as isolated chains. When an external deformation is applied, it is very difficult for the chain segments to establish favorable side-side interactions with neighboring chains, given the random distribution of the network nodes and the segment lengths. Thus, the intermolecular interactions will be independent of deformation. Therefore, the energy accumulated through deformation will be entirely associated with a decrease in conformational entropy, as stipulated by the theory of rubber elasticity [Treloar (1975)].

Astarita and co-workers [Astarita (1974); Astarita and Sarti (1976a, 1976b); Sarti and Esposito (1977) set the basis for what it is known today as the theory of *Purely Entropic Elasticity* (PEE) as applied to polymeric liquids, and have made the assumption that the internal energy of a polymeric fluid is a unique function of temperature, thus independent of deformation. This assumption is tantamount to that of TRE, in that all of the free energy change under deformation is attributed to entropic effects. Mathematically, this assumption is expressed as

$$\hat{U} = \hat{U}(T), \tag{10}$$

and the immediate consequence of this functional relationship is that the constant volume heat capacity per unit mass, defined in the usual fashion as the derivative of the internal energy with respect to temperature at constant density, will also be independent of deformation:

$$\hat{c}_v = \frac{d\hat{U}(T)}{dT}. \tag{11}$$

Based of the assumption of PEE, the energy conservation equation, (4), can be greatly simplified and can be written in the same form as for an isotropic fluid as

$$\rho \hat{c}_v \frac{DT}{Dt} = -\nabla \cdot \mathbf{q} - p\nabla \cdot \mathbf{v} + \tau : \nabla \mathbf{v}. \tag{12}$$

This is a more useful form of Eq. (4) from a practical perspective, since it is expressed in terms of temperature, an easily measurable quantity. It bears reiteration that Eq. (12) is exactly the same as for an isotropic fluid, and it contains no explicit information related to the internal structure or conformation of the fluid, except only indirectly through the extra stress tensor.

When the theory of purely entropic elasticity was applied to polymer melts, its proponents attempted to verify it experimentally. In their experimental procedure, the temperature increase due to viscous heating for planar shear flow and uniaxial elongational stretching was measured [Astarita and Sarti (1976a); Sarti and Esposito (1977)]. Two different polymers were tested: polyisobutylene (PIB) and polyvinylacetate (PVA). From a theoretical perspective, they simplified the heat equation, (4), by assuming a PEE fluid, by neglecting heat conduction effects, and by considering the fluid as homogenous. They subsequently solved Eq. (12) for the heat capacity in the transient regime. Under the experimental conditions, only PIB was found to be purely entropic in nature, while PVA was not. For PIB, the heat capacity was found to converge to the same value for all deformation rates investigated, thus concluding that Eq. (12) was obeyed, and that the PEE assumption used to derive it was reasonable.

In spite of the apparent success of PEE when applied to PIB, there are two main reasons why energetic effects were possibly not captured by these early experiments. First, the spectrum of deformation rates employed was too low (up to 2.78 s^{-1} in the shear flow case) to observe a significant degree of orientation in the fluid microstructure. Second, the flow was homogeneous, i.e., there were no spatial gradients in the degree of orientation. In Sec. IV C, a more general form of the temperature equation will be introduced, without making the PEE assumption. It is then apparent that there is an extra heat generation term arising from the spatial gradients of the degree of orientation. In Sec. II C, there is a detailed explanation as to why a steady-state, homogeneous flow (with respect to the conformation tensor) will cancel out the additional heat generation term that arises when one does not introduce the PEE assumption. It is also possible that the interpretation of Astarita *et al.* for the PVA experimental results was inconclusive as well. The evidence provided only suggests that PVA has a different transient behavior than PIB. The authors did not show clear evidence that the heat capacity is constant with respect to deformation rate, as they did in the PIB case. Venerus (2006) has also recently called these experimental conclusions into question.

However questionable these results were, they established the assumption of PEE as universally applicable in nonisothermal polymer rheology. We are aware of no further attempts to prove or disprove this assumption experimentally.

C. Theoretical Deviations from the Theory of Purely Entropic Elasticity

Virtually all engineering analyses and commercially available software for modeling nonisothermal flow of polymeric fluids use Eq. (12) to describe the temperature evolution of the system. As Astarita (1974) stated explicitly, the theory of PEE has limitations:

> "The implications of this conclusion are very important in the engineering analysis of such polymer processing operations as extrusion and injection molding, where frictional heating is a crucial phenomenon. Polymer melts are known to be nonlinear viscoelastic materials, and unless the assumption embodied in [Eq. (10) in this article] is made, their frictional heating behavior *would not* be described by [Eq. (12) in this article]."

But what is the complete form of the temperature evolution equation if one does not make the assumption that the free energy is purely entropic in nature? First, it is necessary to consider that, aside from temperature, the internal energy of the fluid must have an explicit dependence on one or more internal structural variables. The most widely used quantity to describe the internal structure of a polymer melt is the conformation tensor, **c**, which is defined as the second moment (dyadic product) of the end-to-end vector, **R**, taken as an ensemble average:

$$\mathbf{c} \equiv \langle \mathbf{RR} \rangle. \tag{13}$$

If we consider both temperature and conformation tensor functionalities of the internal energy (for an incompressible fluid),

$$\hat{U} = \hat{U}(T, \mathbf{c}), \tag{14}$$

the constant volume heat capacity per unit mass will be defined as the partial derivative of the internal energy with respect to temperature, at constant **c**:

$$\hat{c}_v = \left. \frac{\partial \hat{U}}{\partial T} \right|_{\mathbf{c}}. \tag{15}$$

Furthermore, the substantial time derivative of the internal energy found on the left side of Eq. (4) becomes [Edwards and Beris (1991a, 1991b); Beris and Edwards (1994)]

$$\frac{D\hat{U}}{Dt} = \hat{c}_v \frac{DT}{Dt} + \left. \frac{\partial \hat{U}}{\partial \mathbf{c}} \right|_T : \frac{D\mathbf{c}}{Dt} = \hat{c}_v \frac{DT}{Dt} + \left. \frac{\partial \hat{U}}{\partial \mathbf{c}} \right|_T : \left(\frac{\partial \mathbf{c}}{\partial t} + \mathbf{v} \cdot \nabla \mathbf{c} \right). \tag{16}$$

The complete form of the temperature evolution equation is thus

$$\rho \hat{c}_v \frac{DT}{Dt} = -\nabla \cdot \mathbf{q} - p \nabla \cdot \mathbf{v} + \boldsymbol{\tau} : \nabla \mathbf{v} - \rho \left. \frac{\partial \hat{U}}{\partial \mathbf{c}} \right|_T : \left(\frac{\partial \mathbf{c}}{\partial t} + \mathbf{v} \cdot \nabla \mathbf{c} \right). \tag{17}$$

It is immediately evident that an additional term appears on the right side of Eq. (17) which does not appear in Eq. (12). This term contains the structural information missing from Eq. (12). In order to evaluate this term, one has to invoke a viscoelastic model, such as the UCMM, to relate the conformation tensor **c** to the rate of strain tensor. In Sec. IV, Eq. (17) will be discussed in detail, and the relative importance of this additional term will be assessed using the UCMM and the single-mode Giesekus model [Giesekus (1982)]. Note that, by a careful choice of the flow system conditions, this term can be made to vanish. For example, if one is interested in a steady-state ($\partial \mathbf{c} / \partial t = 0$), homogenous flow ($\nabla \mathbf{c} = \mathbf{0}$), then Eq. (17) takes the same form as Eq. (12). However, in this case, the heat capacity is no longer independent of deformation rate, as PEE would suggest—see Eqs. (14) and (15).

Two theoretical studies have recently brought the validity of PEE into question [Wapperom and Hulsen (1998); Dressler *et al.* (1999)]. Using the UCMM, a new temperature evolution equation was derived without using the PEE assumption. The new temperature equation has additional terms not appearing in Eq. (12), and includes terms describing the

relaxational fluid processes. Furthermore, the heat capacity is written as a sum of two terms: one that is the equilibrium heat capacity, $\hat{c}_0$, and an explicit contribution from the conformational structure of the polymer,

$$\hat{c} = \hat{c}_0 - \frac{1}{2}\gamma T(\mathrm{tr}\mathbf{c} - \mathrm{tr}\mathbf{c}_0)\frac{\partial^2 K(T)}{\partial T^2}. \tag{18}$$

In this expression, γ is a material constant related to the degree of elasticity per unit mass, $K(T)$ is the (temperature-dependent) overall chain Hookean spring constant, $\mathbf{c}$ is the conformation tensor in the deformed state, and $\mathbf{c}_0$ is the conformation tensor in the unperturbed state. Furthermore,

$$K(T) = \frac{3k_BT}{\langle R^2\rangle_0} = \mu k_BT, \tag{19}$$

where $\langle R^2\rangle_0$ is the mean-squared end-to-end distance of the polymer chains and μ is the conformation tensor normalization factor [Dressler (2000)].

As described by Beris and Edwards (1994), $K(T)$ originated from early statistical models of chain molecules, and was taken as a linear function of temperature (i.e., μ was taken as independent of temperature), under the assumption that the internal free energy of an ensemble of polymer chains was purely entropic in nature. Later, this assumption was removed, and an energetic component to the free energy was identified based upon the nonlinearity of $K(T)$ with respect to temperature [Dressler *et al.* (1999)]. Moreover, the same study identified a configurational contribution to the heat capacity [see Eq. (18)], which was possibly the first theoretical suggestion that the heat capacity of a polymeric liquid changes with degree of orientation.

The temperature dependence of μ was introduced by Gupta and Metzner (1982) through an extra term in their constitutive equation to account for nonisothermal effects

$$\mu = \nu T^{-(B+1)}, \tag{20}$$

where ν and B are fitting constants. Gupta and Metzner pointed out that B is a number greater than -1, and ν is a positive constant. With B greater than -1, μ will decrease with decreasing temperature, and $\langle R^2\rangle_0$ will increase with temperature. A recent simulation study suggests the opposite effect [Ionescu *et al.* (2007)]; however, the simulation results are in good quantitative agreement with data reported by Ciferri *et al.* (1961) for cross-linked polyethylene at 140 °C ($\partial \ln\langle R^2\rangle_0/\partial T = -1.1\cdot 10^{-3}$ K^{-1}). By combining Eqs. (19) and (20), and then taking the derivative with respect to temperature, one obtains $B = -1.45$ from the data of Ciferri *et al.*

It is important to note that Eq. (18) was derived assuming the UCMM, and that if $K(T)$ is a linear function of temperature, then the second term on the right side of Eq. (18) vanishes. However, simulation results seem to indicate that $K(T)$ is not a linear function of temperature, and the conformational contribution to the heat capacity can thus be significant at large deformations [Ionescu *et al.* (2007)]. Furthermore, it is worth emphasizing that the functional form of Eq. (18) is based upon the relatively simplistic UCMM. Other more physically realistic models would produce different functional forms for this physical property.

The heat capacity represents the amount of heat necessary to raise the temperature of a unit mass of an object by one unit of temperature. This amount of heat is directly related to the degrees of freedom of the smallest components (atoms) of that particular object. When a polymeric material is subjected to deformation, the macromolecular chains tend to align on average relative to the direction of the deformation, which results

in a decrease of the total number of degrees of freedom for the chains, or, in other words, a reduction in the heat capacity. Therefore, one would expect that the heat capacity for an aligned system of macromolecules would be always smaller than the quiescent state value; indeed this would evidently always be the case under any applied deformation, regardless of substance. Indeed, as demonstrated later in Sec. IV C, the heat capacity decreases as the deformation rate increases for the model polymer (polyethylene) under consideration herein.

The remainder of the article is organized as follows. In Sec. III, the experimental results of Astarita and co-workers [Astarita (1974); Sarti and Esposito (1977)] are expanded for polyethylene subjected to uniaxial extensional flow under more stringent deformational conditions. In Sec. IV, the generalized form of the temperature equation, (17), is discussed in greater detail, and two simple viscoelastic models are used to evaluate the conformation dependent terms. In Sec. V, a summary of conclusions is presented.

III. EXPERIMENTAL TESTING OF PEE

A. Description of the Experimental Methodology

There are two common steady-state rheological characterization flows, which are inherently different: shear and elongational. Common steady-state shear flow devices currently enjoying widespread use are the cone-and-plate rotational rheometer and the capillary rheometer. Although the cone-and-plate device has the advantage over the capillary of generating a homogenous flow field, the range of shear rates that can be explored is too low to produce the degree of orientation necessary to produce energetic elasticity effects. Of the two, only the capillary viscometer has a high enough shear rate range to allow for the possibility of imposing the large deformations required to see measurable energetic effects. Recall that the shear experiments of Sarti and Esposito (1977) used a rheometer that could not explore shear rates high enough to produce a significant degree of orientation.

Thus experiments were begun using capillary viscometers with the idea in mind to measure the temperature increase over the capillary length for polymeric liquids under very high shear rates. These experiments were ultimately discontinued for two reasons. First, the high end of the shear rate regime that could be generated under the operating conditions of the experimental apparatus, described below, was still too low to generate a large enough degree of orientation to observe energetic phenomena. Second, in the inhomogeneous shear flow through a capillary, the highest shear rates are very near to the capillary wall. Consequently, much of the temperature rise generated by the conformational rearrangements was quickly conducted out of the fluid and into the die. This made measuring an average temperature at the capillary exit prone to large error since the temperature increase was rather small and concentrated near the die wall, rather than in the center of the tube.

On account of the above reasons, the experimental program of research reported herein focused on elongational flow. While the experimental techniques for determining the shear viscosity as a function of deformation rate are very well established, elongational viscosity instruments are still largely in the developmental stage and subject to some controversy. This is due to an array of technical difficulties encountered in these flows, which include the difficulty of generating a controlled, homogeneous, steady-state elongational flow field, combined with the contamination of the flow field by shear effects.

In extensional rheometry, there are two basic techniques for determining the elongational viscosity: tensile testing methods and converging flow methods. Each of these two

methods carries advantages and limitations. The most widely used devices for the direct measurement of the elongational viscosity are the Meissner-type rheometers [Meissner (1972), (1985); Meissner and Hostettler (1994)]. In these devices, the polymer sample is placed between two pulling devices and typically rests atop an oil bath in order to control the temperature and support the sample. The constant elongational rate is achieved by deforming the sample with an exponentially increasing force. In this case, the advantages include the ability to generate shear-free uniaxial, biaxial, and planar elongational flows. Some of the disadvantages include the fact that the sample needs to be very viscous or viscoelastic, typically close to the melting point. Therefore, these devices are limited in the temperature and strain rate ranges, which are usually much lower than the industrial processing conditions they are trying to imitate. Of course, an elongational flow field can be expected to generate much more orientation than a shear flow, at comparable strain rates. However, the Meissner-type devices only function up to Hencky strains of about 3 or 4, and strain rates of about 1 s^{-1}. Thus, once again, in the elongational experiments of Astarita and Sarti (1976a) and Sarti and Esposito (1977), it is highly unlikely that sufficient orientation was induced to notice significant energetic flow phenomena. For large deformations, these experiments suffered from the usual elongational flow problems associated with surface distortion and rupture at large deformations and deformation rates.

The second category of experimental techniques for determining the elongational viscosity is represented by the converging flow methods. See Feigl *et al.* (2003) for a recent discussion of these methods. One of the more controversial methods for determining the elongational viscosity is the semihyperbolically converging die (SHCD) of Collier and co-workers [Collier (1994); Collier *et al.* (1998); Petrovan *et al.* (2000); Feigl *et al.* (2003)].

Much of the controversy of the SHCD has been exaggerated; however, there are some key issues that must be discussed and understood before proceeding further with the experimental analysis. As shown by Feigl *et al.* (2003), it is highly unlikely that a typical polymer melt will acquire a Lagrangian steady state within this device, due to its intrinsically large relaxation time. Consequently, steady state is only achieved in an Eulerian sense. Thus, at best, only an "effective" elongational viscosity can be measured with this device at steady state. However, it has been demonstrated that fairly accurate *transient* "true" elongational viscosity data could be generated under some conditions [Edwards *et al.* (2005)], although this was far from a universal occurrence. Furthermore, Feigl *et al.* demonstrated that a fully uniaxial flow field could only be generated within these dies if there were "full-slip" boundary conditions active at the die wall. In the case of the usual "no-slip" boundary condition, the elongational flow was contaminated by a shear boundary layer near the die wall. Even in this case, however, the flow field and pressure drop were dominated by elongational characteristics, and the average strain rate across the die radius at any axial location maintained the expected value of the elongational strain rate under all conditions. The advantages of these dies are that high strains (up to Hencky values of 7) and strain rates (up to 1000 s^{-1}) can be achieved, thus producing a very large degree of orientation (Kamerkar and Edwards, 2006) within the samples. Furthermore, the confined nature of the flow field prohibits any distortions cause by free surface flow anomalies and sample rupture, and allows higher temperatures to be explored.

There is some evidence suggesting that full-slip boundary conditions are relevant to these dies [Edwards *et al.* (2005); Kamerkar and Edwards (2006)]; however, the issue is irrelevant at present, because in the following analysis, both boundary conditions, full-slip and no-slip, are employed, and the results, as demonstrated below, are qualitatively identical. Consequently, there is no reason to doubt the veracity of the experimental results reported below, regardless of one's perspective on the utility of these dies for

TABLE I. Material characteristics of the polymer samples used in the experiments.

Material	Grade	Melt flow index (g/10 min)	Density (g/cm^3)	Thermal conductivity ($Wm^{-1}\ K^{-1}$)	MW	Polydispersity index
LDPE	Exact 3139	7.5	0.901	0.3	56 950	1.99
HDPE	Paxxon AB40003	0.3	0.943	0.5	105 200	9.74

measuring elongational viscosity. In this study, use is made of the die's ability to generate a flow field with a high elongational strain and strain rate, whether or not that flow field is contaminated by the presence of shear effects near the die wall.

The elongational characteristics of the SHCDs are produced according to their unique geometrical design that incorporates the hyperbolic contours of the streamlines, in which the radius, r, at any axial location, z, is given by the expression

$$r(z) = \sqrt{\frac{\Omega}{z + \Pi}}, \tag{21}$$

In Eq. (21), Ω and Π are geometrical constants,

$$\Omega = L\frac{R_0^2 R_e^2}{R_0^2 - R_e^2}, \tag{22}$$

$$\Pi = L\frac{R_e^2}{R_0^2 - R_e^2}, \tag{23}$$

where L is the length of the die, and R_0, R_e are the entrance and exit radii, respectively. The SHCDs are thus characterized by the Hencky strain number, ε_H, which is the natural logarithm of the ratio of the entrance and exit areas,

$$\varepsilon_H = \ln\left(\frac{A_0}{A_e}\right) = \ln\left(\frac{D_0^2}{D_e^2}\right), \tag{24}$$

where D_0 and D_e are the entrance and exit diameters, respectively. Feigl *et al.* (2003) have demonstrated that the nominal Hencky value of a given die is equivalent to the amount of Hencky strain imparted to an infinitesimal fluid element by the elongational flow field as it passes through the die.

B. Materials

Polyethylene was chosen as the polymer for study, primarily due to its importance in the polymer processing industry. Experiments were conducted on both a low-density (LDPE) and a high-density (HDPE) version, with very different material characteristics, as listed in Table I.

The thermal conductivity of polyethylene usually takes values in the interval $0.2 < k < 0.5\ Wm^{-1}\ K^{-1}$ [Hansen and Ho (1965); Choy *et al.* (1978); Wallace *et al.* (1985); Bird *et al.* (1987)]. Generally, low-density polyethylenes assume values toward the lower limit of the interval, while high-density polyethylenes display values toward the upper limit. For the two polymers considered in this study, exact measurements of the thermal conductivity were not performed. The lower and upper limits of the interval have been

assumed for LDPE and HDPE, respectively. Sensitivity tests conducted using $k = 0.5 \pm 0.25$ Wm^{-1} K^{-1} (employing the finite element methodology to be discussed in Sec. III D) revealed only a 1 °C shift in the predicted exit temperatures, far less than the values measured experimentally.

C. Elongational Viscosity Measurements

In Sec. III A, the possibility of generating a uniaxial elongational flow field under strictly controlled experimental conditions using SHCDs was discussed. This represents an improvement over the original experiments reported in support of PEE by Astarita and co-workers [Astarita and Sarti (1976a); Sarti and Esposito (1977)] in the sense that much higher levels of orientation can be achieved using the SHCDs [Kamerkar and Edwards (2006)]. Here, the objective is to perform similar tests as in the original experiments of Astarita *et al.*, but for higher deformation rates, and thereby also for higher degrees of orientation.

The temperature evolution equation for an incompressible fluid under the PEE assumption is

$$\rho \hat{c}_v \frac{DT}{Dt} = -\nabla \cdot \mathbf{q} + \tau : \nabla \mathbf{v}. \tag{25}$$

The strategy employed herein is to solve this equation numerically for the temperature using as few simplifying assumptions as possible. This will provide the expected temperature rise due to the heat generation term in Eq. (25) (the second term on the right side) over a range of deformation rates. Note that the heat capacity in the above expression is a function of temperature only, and does not depend on conformation. Next, the temperature rise due to heat generation under the same flow conditions is measured experimentally, and then a comparison can be made with the ΔT predicted from the numerical calculations. If the measured temperature rise is in agreement with the calculated one over the entire range of deformation rates, then the assumption of PEE would be verified.

The first step of this strategy is to evaluate the heat generation term ($\tau : \nabla \mathbf{v}$) on the right side of Eq. (25). According to Feigl *et al.* (2003), this term is given by

$$\tau : \nabla \mathbf{v} = \frac{3}{2} \tau_{zz} \dot{\varepsilon} = \frac{\Delta P \dot{\varepsilon}}{\varepsilon_H} = \eta_{ef} \dot{\varepsilon}^2, \tag{26}$$

$$\eta_{ef} = \frac{\Delta P}{\varepsilon_H \dot{\varepsilon}}, \tag{27}$$

where τ_{zz} is the normal stress in the direction of the flow, $\dot{\varepsilon}$ is the elongation rate, ΔP is the pressure difference between the entrance and the exit of the die, and η_{ef} is the effective elongational viscosity. Therefore, in order to evaluate the heat generation term, it is necessary to measure the (Eulerian) steady-state pressure drop, ΔP, as a function of elongation rate. These measurements were conducted using the Advanced Capillary Extrusion Rheometer, manufactured by Rheometrics Inc., after replacing the standard, straight-walled capillary die with an SHCD with a Hencky strain value 6.

In Fig. 1, the effective elongational viscosity is plotted for HDPE [Fig. 1(a)] and LDPE [Fig. 1(b)] at strain rates in the range $2 < \dot{\varepsilon} < 50$ s^{-1}. The measurements were conducted at three temperature set points for each polymer, which corresponded to the inlet temperature at the die entrance, T_{in}. For LDPE, the measurements were performed at 150, 170, and 190 °C, while for HDPE the measurements were performed at 190, 210,

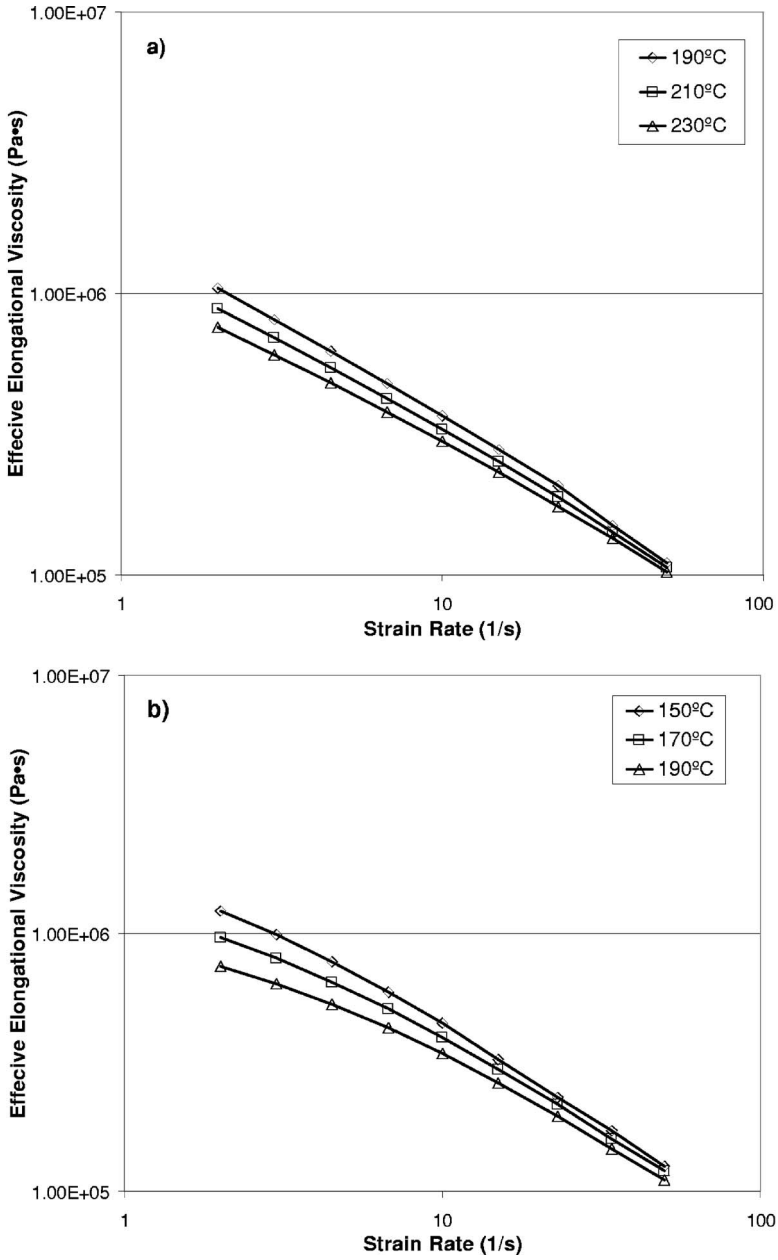

FIG. 1. Effective elongational viscosity vs. strain rate for (a) HDPE and (b) LDPE.

and 230 °C. The upper limit of the temperature interval was dictated by the thermal stability of the polymers, since changes were observed in the color of the polymers from translucent to light brown upon further increase of temperature. High-density polyethylene exhibited a higher thermal stability than LDPE, as expected. The lower limit of the temperature interval was dictated by the physical limit of the pressure transducer. It is well known that the viscosity of a fluid is a strong function of temperature, and it increases as the temperature is decreased. Consequently, the pressure drop recorded by

TABLE II. Arrhenius fitting parameters for the viscosity of HDPE and LDPE.

	HDPE		LDPE	
$\dot{\varepsilon}$ (1/s)	η_0 (Pa s)	A_0/k_B (K)	η_0 (Pa s)	A_0/k_B (K)
2	20 315.723	1834.177	4141.544	2420.944
3	23 065.660	1656.095	6997.973	2106.395
4.5	25 873.061	1481.147	10 712.899	1821.999
6.75	27 098.328	1336.516	15 810.890	1542.317
10	27 646.919	1205.008	20 286.351	1318.180
15	27 491.897	1079.504	30 646.385	1005.090
23	25 539.599	974.864	32 226.460	842.302
34	39 019.108	628.583	27 349.012	783.112
50	43 942.717	430.121	31 115.282	594.244

the pressure transducer will increase as the temperature is lowered for a particular flow rate, which in turn puts limitations on the upper boundary of the strain rate range that can be investigated. We observed that the safety limit of the pressure transducer (56 MPa) was approached at the highest flow rates as the temperature was lowered below the aforementioned limits.

The purpose of measuring the elongational viscosity at different temperatures is twofold. First, it allows testing of the PEE assumption at more than one temperature. Second, the viscosity data at a given elongation rate can subsequently be fitted to an Arrhenius-type expression [Dressler *et al.* (1999)],

$$\eta(T) = \eta_0 \exp\left(\frac{A_0}{k_B T}\right), \tag{28}$$

where η_0 is the "infinite temperature" viscosity and A_0 is an activation energy. This functional form and the fitting parameters η_0 and A_0 at a particular value of the strain rate are then input into the finite element method, discussed momentarily, and account for the temperature dependence of the viscosity. In Table II, the fitting parameters are displayed for both of the polymers investigated in this study.

D. Finite Element Modeling

The heat generation term in Eq. (26) can be determined from the experimental measurements described above, so the next step in the analysis is to compute the radial and axial temperature profiles inside the die channel under flow. This is accomplished by solving Eq. (25) at steady state using as few limiting assumptions as possible.

For this system, the steady-state temperature distribution equation can be written as

$$\rho \hat{c}_v (\mathbf{v} \cdot \nabla T) = k \nabla^2 T + \tau : \nabla \mathbf{v}. \tag{29}$$

Given the complex nature of this partial differential equation, unless highly restrictive assumptions are made, it is not possible to solve it analytically. There is an analytical solution to this equation by assuming an adiabatic system (by effectively zeroing the conduction term $k\nabla^2 T$) and by considering the temperature gradient as having a nonzero component in the axial direction only,

$$\Delta T = T_{exit} - T_{in} = \frac{\Delta P}{\rho \hat{c}_v}. \tag{30}$$

However, this level of approximation produced a severe over-prediction of the actual temperature increase along the die channel. Therefore, it was necessary to obtain a fully numerical solution to this equation, without the abovementioned simplifications, using a finite element (FE) technique. At this point, it is worth emphasizing that Eq. (28) has the assumption of PEE embedded in it, in the sense that it does not contain the term dependent on the internal structure of the fluid—see Eq. (17).

The software package FEMLAB® (v3.0) was used to find numerical solutions to Eq. (29) for various inlet temperatures, elongation rates, and the polymers listed in Table I. The program module was based on the "Steady-State Convection and Conduction" model in the Chemical Engineering module, using two-dimensional axially symmetric space. The temperature functionality of Gaur and Wunderlich (1981) and Brandrup *et al.* (1999) was incorporated into the heat capacity for generic polyethylene, and into the elongational viscosity from the experimental measurements described above. The velocity field is user defined, and constitutes an input variable which defines the convection term on the left side of Eq. (29). The velocity field profile used in this study was previously calculated as [Feigl *et al.* (2003)]

$$v_r = -\frac{1}{2}\dot{\varepsilon} r, \tag{31}$$

$$v_z = \dot{\varepsilon} z. \tag{32}$$

As discussed by Feigl *et al.*, this velocity profile corresponds to a purely uniaxial elongational field. In the present study, it was verified that the velocity profile is that of Eqs. (31) and (32) by solving the momentum equation, (2), independently in a separate set of FE calculations, using the same full-slip boundary conditions. (The effects of the boundary conditions are explored further in Sec. III G.) In the FE analysis, Eq. (29) was solved numerically using the following set of boundary conditions:

1 . At the die entrance, $T(r, z = 0) = T_{in} = T_{set}$; (33)

2 . At the wall, $T\left(r = \sqrt{\frac{\Omega}{z + \Pi}}, z\right) = T_{set}$. (34)

The FE calculations provided the radial and axial temperature profiles inside the die channel, which allowed computation of the average temperature values over the exit cross section of the die. The Hencky strain number for the die used in these calculations was 6 [see Eq. (24)], the same as in the experimental measurements. This particular Hencky value was determined as the best compromise between the desired production of a high degree of orientation, and the practical necessity of having a reasonably large exit diameter over which to calculate an average temperature. The FE calculations enabled the prediction of an effective temperature increase due to heat generation throughout the die as

$$\Delta T = \langle T \rangle_{exit} - T_{in}, \tag{35}$$

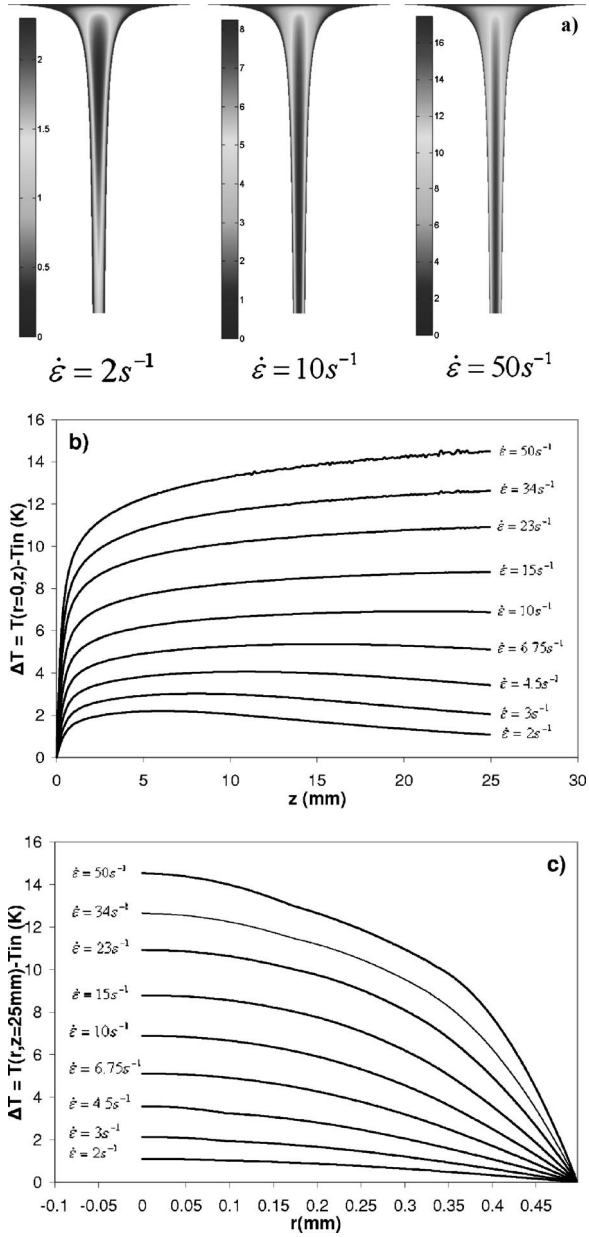

FIG. 2. The temperature distribution within the SHCD, (a), as well as the (b) axial and (c) radial temperature profiles for HDPE at T_{in}=190 °C.

$$\langle T \rangle_{exit} = \frac{\int_0^{R_e} T(r, z = L) r dr}{\int_0^{R_e} r dr}. \tag{36}$$

In Fig. 2(a), the temperature distribution throughout the SHCD is displayed, where the

red end of the visible spectrum denotes higher temperatures, and the blue end denotes cooler ones. This graphic conveys the basic ideas that the temperature increases axially down the die, and decreases near the wall. The axial temperature profile at $r=0$ [Fig. 2(b)] and the radial temperature profile at $z=25$ mm [Fig. 2(c)] are presented for the HDPE melt at the inlet temperature of 190 °C in terms of the net temperature increase, $\Delta T=\langle T\rangle_{exit}-T_{in}$, at all elongation rates examined using the FE simulations. In the axial temperature profiles of Fig. 2(b), there is a maximum occurring close to the entrance at the lowest flow rates, due to the simultaneous occurrence of two competing phenomena. First, heat is generated within the body of the fluid. The stresses and the velocity gradients giving rise to the heat generation term are constants with respect to axial and radial position for a particular flow rate [Feigl *et al.* (2003)], which in turn makes the heat generation term a constant throughout the entire spatial domain. Second, heat is removed via conduction through the die wall. The conduction term is not a constant with axial position. As the radius of the channel gets smaller, the heat loss through the die wall increases. The heat conduction term compensates for the generation term, thus reducing the temperature. However, as the flow rate is increased, the maximum in the axial temperature profile will be pushed towards the exit. While the heat conduction term increases slowly with strain rate (due to sharper temperature gradients), the heat generation term is increasing much faster with strain rate, and eventually overwhelms the heat loss through the die wall throughout the entire spatial domain. The radial temperature profiles of Fig. 2(c) are much simpler to understand: the temperature is highest at the center of the die, and decreases dramatically as the die wall is approached, due to the heat conduction through the die wall.

At the die exit, an average value for the temperature can be calculated by numerical integration using Eq. (36). Typically, the average temperature for a cross section [or the "bulk temperature" (Bird *et al.*, 2002)] is also weighted by the axial velocity, v_z. In this case, v_z is independent of the radial position, and will drop out of the equation:

$$\langle T\rangle_{exit}=\frac{\int_0^{R_e}T(r,z=L)v_z r dr}{\int_0^{R_e}v_z r dr}=\frac{v_z\int_0^{R_e}T(r,z=L)r dr}{v_z\int_0^{R_e}r dr}=\frac{\int_0^{R_e}T(r,z=L)r dr}{\int_0^{R_e}r dr}. \tag{37}$$

In Fig. 3, the average temperatures at the exit cross section of the die resulting from the FE calculations are presented for HDPE [Fig. 3(a)] and LDPE [Fig. 3(b)]. For consistency, the temperatures are given in terms of the net change with respect to the inlet temperature. The FE calculation results are not surprising: there is a steady temperature increase as the strain rate is increased for both HDPE and LDPE. This can be explained by considering the heat generation term

$$\tau:\nabla\mathbf{v}=\eta_{ef}\dot{\varepsilon}^2. \tag{38}$$

Even though the viscosity is decreasing as the strain rate increases, the heat generation term is directly proportional to the second power of the strain rate. Overall, the heat generation term will increase almost linearly with strain rate. Moreover, for a given flow rate, the temperature rise will increase as the inlet temperature is decreased. Again, this is a consequence of the generation term, because the viscosity increases as the temperature is decreased. It is worth pointing out that at the same inlet temperature (190 °C), the temperature increase is larger for LDPE than it is for HDPE. This is somewhat counterintuitive, given the fact that the viscosity of HDPE is greater than that of LDPE at the same temperature (see Fig. 1). Nevertheless, this behavior is explained by taking the

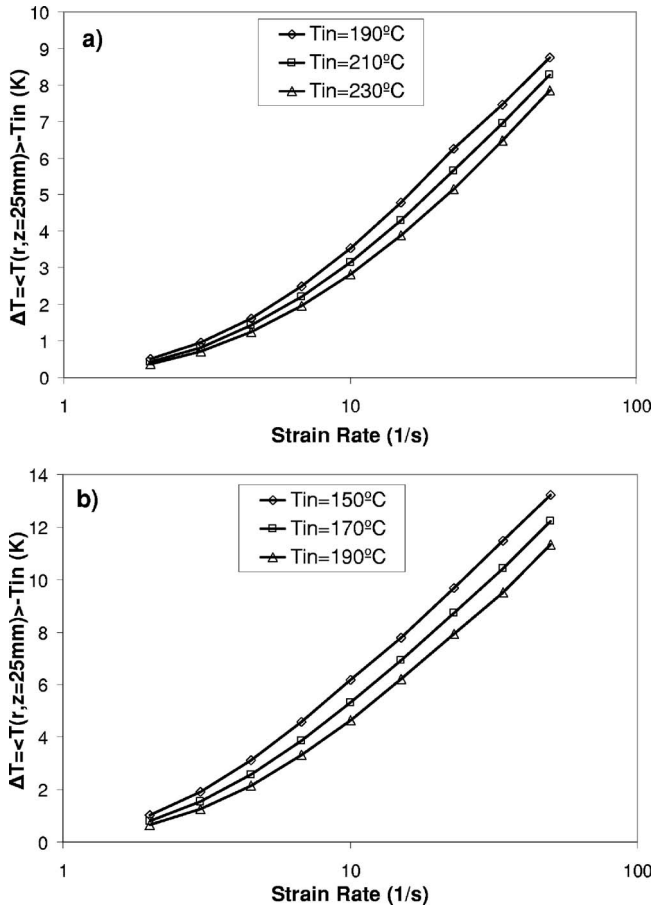

FIG. 3. Calculated average temperature changes at the die exit for (a) HDPE and (b) LDPE.

thermal conductivity into consideration. (In Table I, the thermal conductivity values for typical HDPE and LDPE melts are presented.) In the FE calculations, it is observed that the temperature profiles are marginally sensitive to the thermal conductivity, so the lower value of k for LDPE fully accounts for the abovementioned behavior.

E. Experimental temperature measurements

With the temperature profile calculations completed, measurements were made of the temperature change under the same conditions used in the FE simulations. This was accomplished by placing a thermocouple at the die outlet in order to measure the temperature of the fluid exiting the die at a given flow rate and inlet temperature. A schematic of the experimental design for measuring the outlet fluid temperature is presented in Fig. 4. The entire ensemble was maintained at the fluid inlet temperature. The temperature probe used to measure the temperature of the fluid at the die exit, T_{exit}, was obtained from Omega Engineering Inc. incorporating a J-type iron-constantan thermocouple, with part number JMQSS-032U-6. The temperature readings were made on a DP26-TC Differential Temperature Meter, also obtained from Omega Engineering Inc., with a precision of 0.1 °C. The temperature increase, $\Delta T = T_{exit} - T_{in}$, was recorded as a function of strain rate for various inlet temperatures.

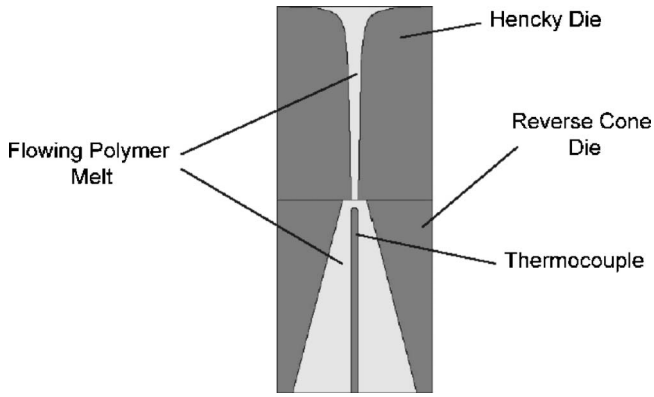

FIG. 4. Schematic of the experimental design for measuring the temperature of the fluid at the die exit.

The complete results for HDPE are presented in Fig. 5. In these experimental measurements, the same qualitative behavior is observed as was predicted by the FE simulations. It is apparent that excellent agreement exists between the simulated and measured values for ΔT at low to moderate elongation rates. However, at high elongation rates, a systematic deviation from the calculated values became increasingly evident. Moreover, as the inlet temperature is decreased, the onset of the deviation occurred at lower flow rates. Note that at the highest strain rate obtainable experimentally, the deviation between the two sets of data was as high as 100%! Note also that the strain rates where the deviation began to manifest were well beyond the attainability of the instruments used by Astarita and co-workers.

In Fig. 6, we compare the behavior of HDPE and LDPE under the same inlet conditions (T_{in}=190 °C). Notice that the agreement between the measured and predicted temperature changes for LDPE is maintained for a wider range of elongation rates. As discussed later, this is due to differences in the relaxation times between the two poly-

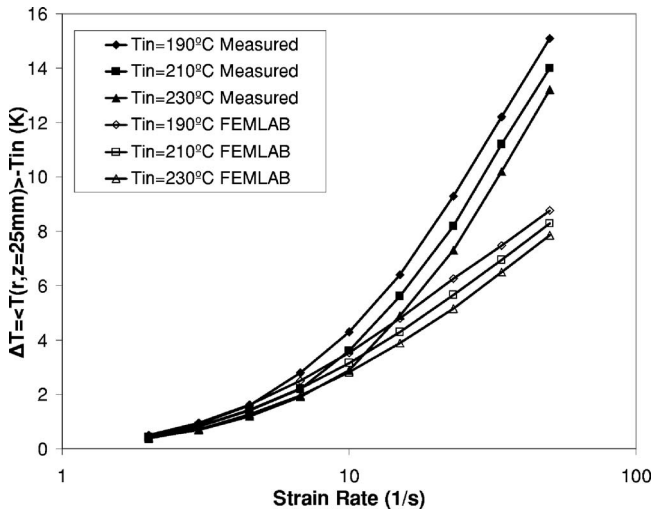

FIG. 5. Temperature changes for HDPE: filled symbols represent the measured values; open symbols represent the simulated FE values.

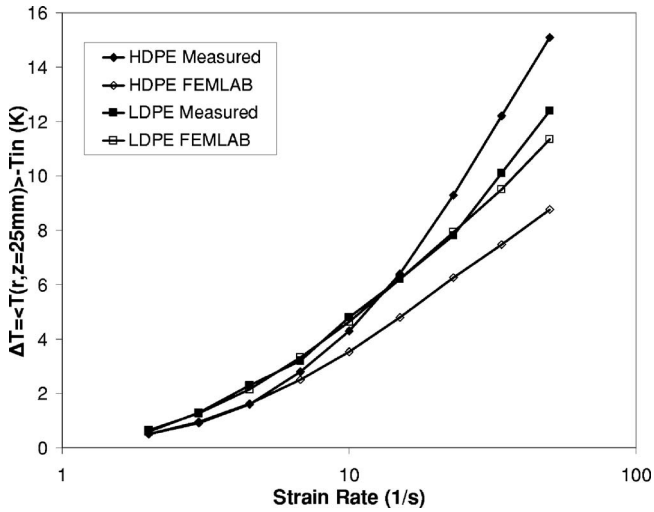

FIG. 6. Measured (filled symbols) and calculated (open symbols) temperature changes for HDPE (diamonds) and LDPE (squares) at $T_{in}=190\,^{\circ}\mathrm{C}$.

mers. Clearly, both polymers investigated show deviations from the predicted temperature profiles to various degrees. This is clear evidence that Eq. (29) is not obeyed for the entire range of elongation rates employed in this study. Henceforth, it is necessary to try to find possible explanations as to why deviations from Eq. (29) are observed.

F. Theoretical analysis

It is necessary to examine the temperature distribution dictated by Eq. (29), and also the assumptions that were made in deriving and solving it. The analysis started with the energy balance of Eq. (4)

$$\rho\frac{D\hat{U}}{Dt}=-\nabla\cdot\mathbf{q}-p\,\nabla\cdot\mathbf{v}+\tau:\nabla\mathbf{v}. \tag{39}$$

The following assumptions were made:

1. The fluid is incompressible $(\nabla\cdot\mathbf{v}=0)$; (40)

2. The flow is steady in an Eulerian sense $\left(\frac{\partial\hat{U}}{\partial t}=0 \text{ and } \frac{D\hat{U}}{Dt}=\mathbf{v}\cdot\nabla\hat{U}\right)$; (41)

3. The fluid is purely entropic $\left(\hat{U}=\hat{U}(T) \text{ and } c_v=\frac{d\hat{U}(T)}{dT}\right)$; (42)

4. Full-slip boundary conditions apply at the die wall;

5. The thermal conductivity is isotropic.

Certainly, one would expect assumption 1 to apply to liquids for a wide range of pressures. In the experiments, pressures of up to 50 MPa were applied, which is not enough to observe density changes through compression. The second assumption is also

reasonable in this case: sufficient time was allowed during measurements for both the pressure and the temperature to reach steady-state values, as these quantities could be monitored *in situ*. As a direct consequence of the third assumption, the constant volume heat capacity is a constant with respect to elongation rate (i.e., the degree of orientation developed in the melts), so there is no configurationally dependent extra term. For the moment, however, assumption 3 is retained, but it will be called into question later.

Applying the first three assumptions above, the energy balance of Eq. (37) becomes the steady-state temperature distribution equation, (43),

$$\rho \hat{c}_v(\mathbf{v} \cdot \nabla T) = -\nabla \cdot \mathbf{q} + \tau : \nabla \mathbf{v}. \tag{43}$$

Including assumption 4, the heat generation term is given by (Feigl *et al.*, 2003)

$$\tau : \nabla \mathbf{v} = \eta_{ef} \dot{\varepsilon}^2. \tag{44}$$

By applying Fourier's law,

$$\mathbf{q} = -k \nabla T, \tag{45}$$

and, considering the fluid to be isotropic in the sense that heat is conducted in all directions with the same thermal conductivity, the final form of the temperature distribution equation used in our FE calculations is

$$\rho \hat{c}_v(\mathbf{v} \cdot \nabla T) = k \nabla^2 T + \eta_{ef} \dot{\varepsilon}^2. \tag{46}$$

In the next subsections, each of these assumptions is examined in turn.

G. Effect of the Boundary Conditions

The effect of assumption 4 on the simulated temperature profiles was explored by performing a set of FE calculations in which the momentum and heat equations were solved simultaneously as a coupled system of partial differential equations. The full-slip boundary conditions were tested, and yielded identical results to those presented in prior subsections. Then, the full-slip conditions were replaced by no-slip boundary conditions, and the resulting velocity profiles were used to define the convection term on the left side of Eq. (46). The pressure drop maintained its experimental value, thus determining the viscosity coefficient. In this case, the radial and axial components of the velocity field differed significantly from Eqs. (31) and (32) respectively, as demonstrated by Feigl *et al.* (2003).

In Fig. 7, the axial temperature profiles obtained using the full-slip and no-slip boundary conditions are presented for the HDPE melt at $T_{in} = 190$ °C and $\dot{\varepsilon} = 34$ s^{-1}. It is clear from Fig. 7 that changing the boundary conditions has a small but significant quantitative effect on the temperature profile, mainly because the convection term was altered. However, the introduction of the no-slip conditions at the wall lowers the temperature profile, because more of the heat generation occurs in the shear thin boundary layer near the wall, where it can be more quickly conducted out through the die wall. Furthermore, when shear is present, the elongational component of the flow field is reduced, resulting in less polymer orientation and thus a smaller temperature rise. The temperature profile would necessarily have to rise, not decline, for boundary conditions to explain the deviation between the simulated and experimental data. Therefore, the conclusion is that the boundary conditions used in this study (assumption 4) cannot be responsible for the deviations observed in Figs. 5 and 6.

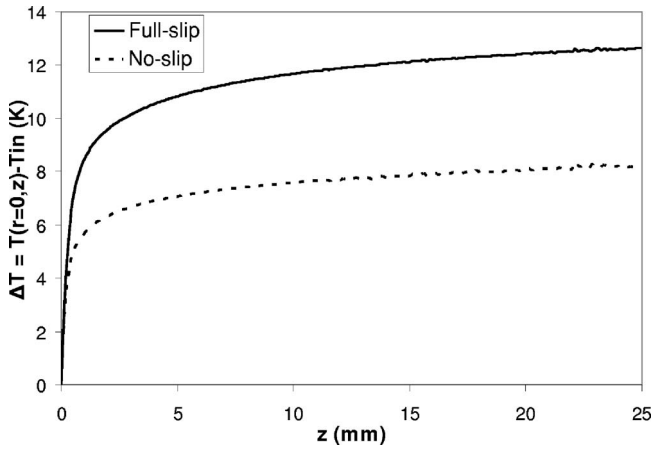

FIG. 7. Effect of the applied boundary conditions on the calculated axial temperature profiles for the HDPE melt at $T_{in}=190\ ^{\circ}\mathrm{C}$ and $\dot{\varepsilon}=34\ \mathrm{s}^{-1}$.

H. Effect of Anisotropic Thermal Conductivity

While the thermal conductivity of polymeric materials at equilibrium is isotropic (i.e., has the same value in all directions), it is well known that for deformed polymers, the thermal conductivity becomes anisotropic [Choy *et al.* (1978, 1993); Hands (1980); Wallace *et al.* (1985); Venerus *et al.* (1999a), (1999b), (2001), (2004); Iddir *et al.* (2000); Kurabayashi (2001); Dai and Tanner (2006)]. This phenomenon can be explained by examining the way in which thermal energy is conducted in oriented polymeric materials. In a polymeric material subjected to deformation, the chains become stretched out and partially aligned with each other. Kinetic theory suggests that the propagation of the thermal vibrations is accomplished more efficiently along the backbone of the chain, because it consists of strong covalent bonds. The van der Waals interactions established between side chains are weaker and longer ranged, which makes it more difficult for the thermal fluctuations to propagate in a direction perpendicular to the polymer chains.

Experimentally, it has been shown that the thermal conductivity in the direction parallel to the direction of deformation ($k_{\parallel}$) increases with degree of orientation, while the thermal conductivity perpendicular to the direction of deformation ($k_{\perp}$) decreases. This phenomenon is highly sensitive to temperature and to the physical state of the polymer. For example, measurements have revealed that when solid high-density polyethylene is subjected to uniaxial extension at room temperature with draw ratios between 1 and 25, $k_{\perp}$ suffers a reduction of up to 50% with respect to the isotropic value, accompanied by a simultaneous increase in $k_{\parallel}$ of up to 2000%, approaching the value for stainless steel [Choy *et al.* (1978)]. In polymer melts subjected to shear or extensional flows, the extent to which the two components of the anisotropic thermal conductivity tensor change is much lower. Notable is the work of Venerus and co-workers, in which they developed a noninvasive method for measuring the anisotropic thermal conductivity in polymer melts under static or dynamic conditions through forced Rayleigh light scattering. Decreases in $k_{\perp}$ of up to 10% and increases in $k_{\parallel}$ of up to 20% were observed during shear [Venerus *et al.* (1999a), (1999b), (2001), (2004); Iddir *et al.* (2000); Balasubramanian *et al.* (2005)] and extensional [Venerus *et al.* (2001)] flows.

In an effort to relate the anisotropic thermal conductivity tensor to the extra stress tensor, van den Brule (1989) suggested a linear relation between the two tensors using a simple network model for polymer liquids,

$$\mathbf{k} - \frac{1}{3}\mathrm{tr}(\mathbf{k})\,\delta = k_{iso} C_t \tau, \tag{47}$$

where k_{iso} is the isotropic thermal conductivity and C_t is called the "stress-thermal coefficient." Equation (47) represents a formulation of the stress-thermal law, which is analogous to the stress-optical law relating the refractive index tensor to the extra stress tensor. Subsequent research has determined that the stress-thermal law is valid for a wide range of polymers and deformations [Venerus *et al.* (1999a, 1999b), (2001), (2004); Balasubramanian *et al.* (2005); Dai and Tanner (2006)].

With this in mind, the effect of changing the thermal conductivity was tested in the FE calculations. Following the recipe reported in literature, the anisotropic conductivity components were set to $k_{\perp} = 0.9 k_{iso}$ and $k_{\parallel} = 1.2 k_{iso}$ for HDPE at $T_{in} = 190\ ^{\circ}\mathrm{C}$, at a strain rate where deviation from the calculated temperature profile was observed ($\dot{\varepsilon} = 34\ \mathrm{s}^{-1}$). It is important to point out that we can only make qualitative assessments at this point, given that the stress-thermal coefficient for HDPE under uniaxial elongational flow has not yet been reported. The most extreme situation reported in literature (10% decrease in $k_{\perp}$ and 20% increase in $k_{\parallel}$) was chosen as the test case in order to prove the point. As described by Feigl *et al.* (2003), the extra stress tensor is constant (after a brief entrance region) throughout the entire spatial domain under full-slip conditions; therefore, the stress-thermal law may prove to be valid in this case as well. However, it has been inferred that the level of orientation achieved within the Hencky dies increases steadily with axial position [Feigl *et al.*, 2003; Kamerkar and Edwards (2006)]. If it is assumed that the anisotropic thermal conductivity is related to the internal degree of orientation, then a more refined expression for the thermal conductivity as a function of axial position could be introduced. Therefore, it is not expected that a quantity which is dependent on the degree of orientation would reach a plateau value either. As seen later on, an exact expression that relates the thermal conductivity tensor to the axial position is not needed, and useful conclusions can be inferred from the general trends observed.

In the FE analysis, the ability exists to specify an anisotropic form for the thermal conductivity. In this specific case, where cylindrical coordinates are used, the anisotropic thermal conductivity is defined by two values: the perpendicular component, k_{rr}, and the parallel component, k_{zz}.

In Fig. 8, the axial temperature profiles are displayed in terms of the temperature change with respect to the inlet temperature for the two cases when the isotropic thermal conductivity (k_isotropic) and the anisotropic thermal conductivity (k_anisotropic) were applied to the HDPE melt. The system conditions are $T = 190\ ^{\circ}\mathrm{C}$ and $\dot{\varepsilon} = 34\ \mathrm{s}^{-1}$. It is evident that even in the most extreme case, changing the thermal conductivity from isotropic to anisotropic has a minimal impact on the calculated temperature profiles. The profiles in Fig. 8 were calculated using constant values for k_{rr} and k_{zz} with respect to axial position. As detailed above, it is expected that those values would change gradually from k_{iso} at the die entrance to a specific value towards the exit, which would make the difference observed in Fig. 8 even less pronounced.

Figure 8 implies that the thermal conductivity is not responsible for the deviations shown in Figs. 5 and 6. It is apparent that even if the anisotropy in k does have an impact in the measurements, it is going to be minimal and in the *opposite direction*; i.e., it tends to decrease the temperature change, rather than increase it. Recent experimental work

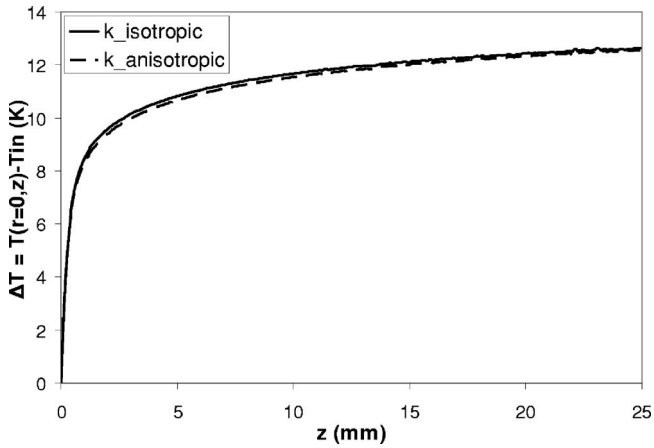

FIG. 8. Effect of anisotropy in thermal conductivity on the axial temperature profile.

[Venerus *et al.* (1999a, 1999b), (2001), (2004)] suggests that the conductivity is related to the plateau modulus of the liquid; this implies that for the plateau modulus of the HDPE used herein, 0.1 MPa, and the measured pressure drops, on the order of 10 MPa, that the window of variation in the components of the conductivity tensor could be ten times larger than those used in the simulations. However, larger variations in the components of the conductivity tensor would only exacerbate further the discrepancy between theory and experiment.

The explanation behind this behavior is not immediately obvious as in the test of the boundary conditions. In this case, there is a competition between two phenomena. First, there is the anisotropic conduction, which transports more of the heat generated in the fluid toward the die exit rather than toward the wall where it could be conducted out of the fluid. Competing against this process is the reduction in the heat generation due to the smaller value of the viscosity at higher temperature. Consequently, as more heat is conducted axially, the temperature increases, inducing a concurrent decrease of the viscosity, and thereby producing less heat generation and lowering the temperature. This competition explains why the computed temperature profiles are only slightly different from each other.

This conclusion is very important in the analysis, because by process of elimination, the only remaining cause for the deviations shown in Figs. 5 and 6 is the third assumption, Eq. (42). Eliminating this assumption has two consequences: first, the heat capacity can no longer be assumed as independent of the degree of orientation, and second, the extra term on the right side of Eq. (17) is potentially important, and can no longer be neglected. This conclusion offers fresh criticism of the validity of PEE under the high strain-rate experimental conditions employed in this study.

IV. GENERALIZED TEMPERATURE EQUATION

A. Conformation tensor evolution equations

Using the UCMM, the time and space evolution equations for the conformation tensor are [Beris and Edwards (1994)]

$$\check{\mathbf{c}} = -\frac{1}{\lambda}\mathbf{c} + \frac{k_B T}{\lambda K(T)}\delta, \tag{48}$$

where $\check{\mathbf{c}}$ is the upper-convected time derivative of the conformation tensor and λ is the relaxation time. The upper-convected time derivative is defined as

$$\check{\mathbf{c}} = \frac{\partial \mathbf{c}}{\partial t} + \mathbf{v}\cdot\nabla\mathbf{c} - \mathbf{c}\cdot\nabla\mathbf{v} - \mathbf{c}\cdot(\nabla\mathbf{v})^T. \tag{49}$$

In Cartesian coordinates, the velocity gradient field developed in the Hencky die corresponding to a uniaxial extension is written as

$$\nabla\mathbf{v} = \begin{pmatrix} -\dot{\varepsilon}/2 & 0 & 0 \\ 0 & -\dot{\varepsilon}/2 & 0 \\ 0 & 0 & \dot{\varepsilon} \end{pmatrix}. \tag{50}$$

In this case, the fluid is extended in the z direction, while it is being contracted in the x and y directions. Consequently, Eq. (49) can be rewritten for the diagonal components of the conformation tensor as

$$\check{c}_{xx} = \frac{\partial c_{xx}}{\partial t} + \dot{\varepsilon} c_{xx}, \tag{51}$$

$$\check{c}_{yy} = \frac{\partial c_{yy}}{\partial t} + \dot{\varepsilon} c_{yy}, \tag{52}$$

$$\check{c}_{zz} = \frac{\partial c_{zz}}{\partial t} - 2\dot{\varepsilon} c_{zz}. \tag{53}$$

The off-diagonal components of the conformation tensor vanish in this flow field. If Eq. (48) is rewritten in terms of the normalized conformation tensor, and combined with Eqs. (51)–(53), the following system of partial differential equations for the diagonal components of the normalized conformation tensor is obtained:

$$\frac{\partial \widetilde{c}_{xx}}{\partial t} = \widetilde{c}_{xx}\left(-\dot{\varepsilon} - \frac{1}{\lambda}\right) + \frac{1}{\lambda}, \tag{54}$$

$$\frac{\partial \widetilde{c}_{yy}}{\partial t} = \widetilde{c}_{yy}\left(-\dot{\varepsilon} - \frac{1}{\lambda}\right) + \frac{1}{\lambda}, \tag{55}$$

$$\frac{\partial \widetilde{c}_{zz}}{\partial t} = \widetilde{c}_{zz}\left(2\dot{\varepsilon} - \frac{1}{\lambda}\right) + \frac{1}{\lambda}. \tag{56}$$

Integrating these expressions, and using Eq. (24) for the definition of the Hencky strain number, ε_H, the following analytical solution of this system of equations is then

$$\widetilde{c}_{xx} = \widetilde{c}_{yy} = \frac{\lambda\dot{\varepsilon}}{\lambda\dot{\varepsilon}+1}\left[\left(\frac{z}{L}\right)^{-(1+1/\lambda\dot{\varepsilon})} \cdot \exp\left[-\left(\frac{t_R}{\lambda} + \varepsilon_H\right)\right]\right] + \frac{1}{1+\lambda\dot{\varepsilon}}, \tag{57}$$

$$\tilde{c}_{zz} = \frac{2\lambda\dot{\varepsilon}}{2\lambda\dot{\varepsilon}+1}\left[\left(\frac{z}{L}\right)^{(2-1/\lambda\dot{\varepsilon})} \cdot \exp\left[-\left(\frac{t_R}{\lambda} - 2\varepsilon_H\right)\right]\right] - \frac{1}{2\lambda\dot{\varepsilon}-1}, \tag{58}$$

where t_R is the residence time of a fluid element within the die (Feigl *et al.*, 2003).

In the case of the single-mode Giesekus model, the conformation tensor evolution equation is [Beris and Edwards (1994)]

$$\overset{\nabla}{\tilde{\mathbf{c}}} = -\frac{1}{\lambda}((1-\beta)\delta + \beta\tilde{\mathbf{c}}) \cdot (\tilde{\mathbf{c}} - \delta), \tag{59}$$

where β is an empirical constant lying in the range [0,1]. When β=0, the UCMM is recovered. For $\beta > 0$, Eq. (59) is quadratic in terms of the conformation tensor components, which makes it more difficult to solve analytically. However, Eq. (59) can be solved numerically using a fourth-order Runge-Kutta method. The parameter β is not known *a priori*, and is typically determined by fitting experimental data. In this study, the Giesekus model will be used to refine the UCMM predictions. Note that the Helmholtz free energy of the Giesekus model is the same as for the UCMM [Beris and Edwards (1990a, 1990b), (1994)], as is the conformational contribution to the heat capacity, Eq. (18) [Dressler *et al.* (1999)].

At this point, everything that is necessary to evaluate the normalized conformation tensor components as a function of axial position and strain rate is at hand, except for the relaxation time. This characteristic time was determined by measuring the dynamic loss and storage moduli for each polymer melt. This was achieved by performing a dynamic frequency sweep using the cone-and-plate geometry of an Advanced Rheometric Expansion System rheometer, manufactured by Rheometrics Inc. At low frequencies, when the loss modulus is greater than the storage modulus, the polymer melt is considered to behave as a viscous fluid, while at high frequencies, the storage modulus is greater, and the material is considered to develop elastic characteristics. The frequency where the two moduli intersect is called the "crossover point," and its reciprocal provides a characteristic relaxation time. The value of λ was measured at various temperature values for each polymer, and the resulting experimental data were used to fit two exponential parameters, A_λ and B_λ, to the functional form

$$\lambda = A_\lambda \exp\left(\frac{B_\lambda}{T}\right). \tag{60}$$

This temperature dependence of λ is displayed in Fig. 9—see Ionescu (2006) for more details concerning the measurements of the relaxation times and moduli. As expected, the relaxation times for both polymers decrease with increasing temperature. Moreover, the relaxation times measured for HDPE are about two orders of magnitude larger than the ones estimated for LDPE; this is not surprising, given the larger molecular weight of HDPE compared to LDPE—see Table I. The fitting parameters of Eq. (60) are presented in Table III.

B. Conformation tensor evolution inside the die channel

With the measured values of the relaxation times, the diagonal components of the conformation tensor can be calculated according to Eqs. (57) and (58) for the UCMM, and by numerically integrating Eq. (59) for the Giesekus model. In this case, it is instructive to use the trace of the normalized conformation tensor as the general descriptor for the degree of orientation achieved. As previously discussed, the strain rate inside the die channel is independent of either axial or radial position under full-slip boundary condi-

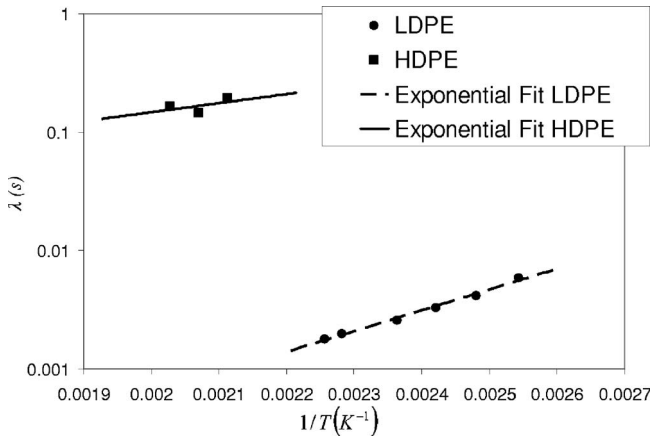

FIG. 9. Temperature dependence of the relaxation times for LDPE and HDPE.

tions. Therefore, no radial dependence of the conformation tensor is expected either. However, as discussed in Sec. III D, there are significant radial temperature gradients inside the die channel, which will definitely have an impact on the radial dependence of the relaxation time. According to Eqs. (57)–(59), the conformation tensor has an explicit dependence on the relaxation time; therefore, it will also have a dependence on the radial position. For simplicity, however, the relaxation time is still taken as a constant throughout the entire spatial domain, with the value calculated for the temperature of the fluid at the die inlet. Under this approximation, the conformation tensor is only a function of axial position.

In Fig. 10, the calculated value of $\mathrm{tr}(\tilde{\mathbf{c}})$ is displayed for the HDPE melt as a function of axial position at $T_{in}=190\ ^{\circ}\mathrm{C}$ for the elongation rates considered in the experiment. For clarity, it is convenient to normalize $\mathrm{tr}(\tilde{\mathbf{c}})$ with respect to its value at the exit ($z=25$ mm). Results are shown for calculations using both the UCMM and the Giesekus model. In the case of UCMM [Fig. 10(a)], the degree of orientation only approaches a constant value at the lowest elongation rates. As the elongation rate increases, the orientation profiles change markedly toward a more steady increase with axial position, which becomes increasingly shifted toward the die exit as the strain rate increases. In the case of the Giesekus model [Fig. 10(b)], the same qualitative behavior is observed as in the UCMM case, but only at the lowest strain rates. At high strain rates, the parameter β acts to limit the growth rate of $\mathrm{tr}(\tilde{\mathbf{c}})$ towards a constant value. As seen later, the value of the parameter β which predicted the closest agreement with the experimental measurements was $\beta=0.0065$.

In Fig. 11, the values of $\mathrm{tr}(\tilde{\mathbf{c}})$ calculated at the die exit using the UCMM are displayed for the HDPE melt at all inlet temperatures and elongation rates. The trace of the conformation tensor (i.e., the degree of orientation) becomes important virtually in the same

TABLE III. Exponential fitting parameters of the relaxation time for HDPE and LDPE.

Polymer	A_λ (s)	B_λ (K)
HDPE	4.422738×10^{-3}	1.753809×10^{3}
LDPE	1.898411×10^{-7}	4.043431×10^{3}

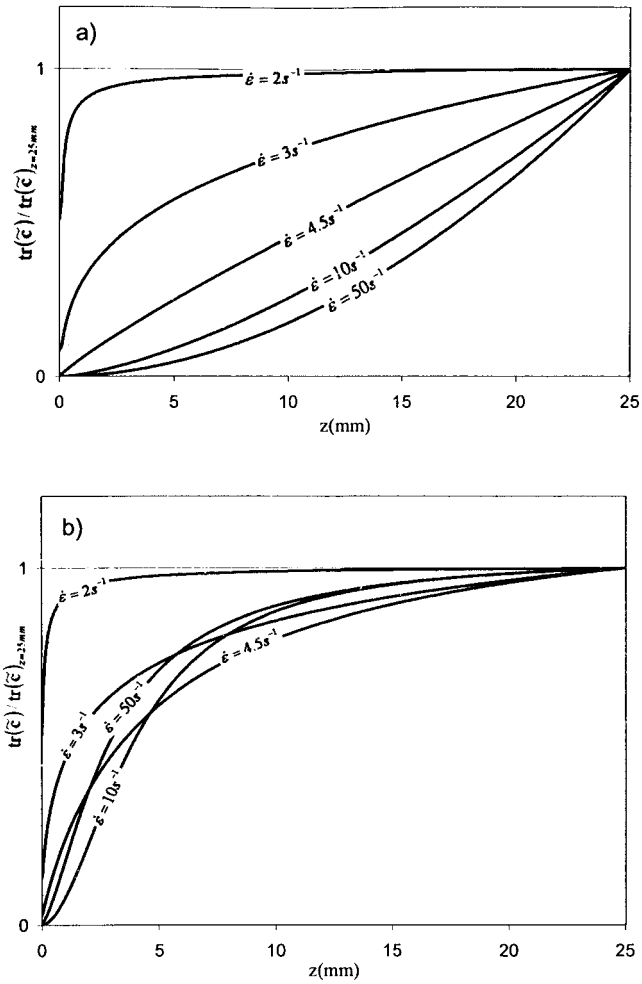

FIG. 10. Axial dependence of the degree of orientation for the HDPE melt at T_{in}=190 °C: (a) UCMM; (b) Giesekus model.

region of the strain-rate range where the deviations occurred in Fig. 5. Furthermore, the influence of the temperature seems to be preserved as well, and the same qualitative behavior with respect to temperature is observed in both figures. This new evidence seems to indicate a definite correlation between the degree of orientation and the region in the strain-rate range where PEE is not valid. It is worth emphasizing that the data in Fig. 11 were generated using the rather simplistic UCMM and the measured relaxation times. Therefore, the relaxation time may prove itself useful in predicting the region where the orientation effects in the energy balance of the system become important.

To emphasize the points made in the previous paragraph, the data in Figs. 5 and 11 are plotted together on the same graph in Fig. 12. The trace of the conformation tensor is with respect to the left ordinate, and is represented by the filled symbols, while the difference between the measured and the calculated temperature changes is represented by the open symbols with respect to the ordinate on the right. The diamond, square, and triangle symbols represent data at inlet temperatures of 190, 210, and 230 °C, respectively. As evident from the figure, the degree of correlation between the two quantities is

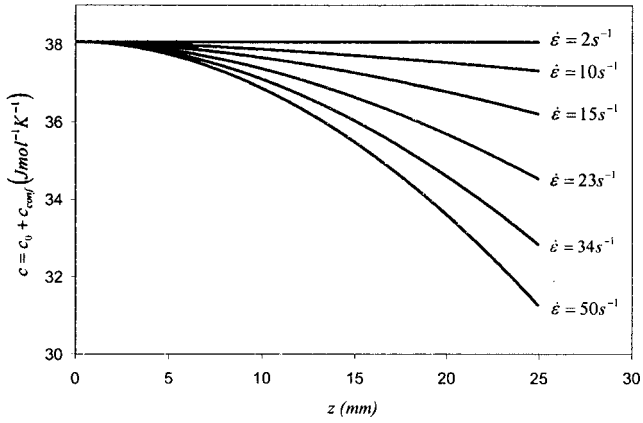

FIG. 11. Strain rate dependence of $\mathrm{tr}(\tilde{c})$ at the die exit for the HDPE melt at T_{in}=190, 210, and 230 °C, calculated using the UCMM.

astounding. Indeed, this correlation calls to mind the stress-thermal law of Eq. (47), since, in the UCMM, stress is linearly proportional to the conformation tensor (Bird *et al.*, 1987; Beris and Edwards, 1994). Moreover, the high degree of correlation suggests a functional form for a conformation dependent temperature. If $U(V,S,\mathbf{c})$ is taken as $U = U_{eq}(S,V) + EU_{eq}(s,V)(\mathrm{tr}\tilde{\mathbf{c}} - 3)$, where E is a dimensionless constant, then thermodynamics implies that

$$T_{NE} = T_{eq} + ET_{eq}(\mathrm{tr}\tilde{\mathbf{c}} - 3). \tag{61}$$

By plotting T_{NE}/T_{eq} versus $\mathrm{tr}\tilde{\mathbf{c}} - 3$ for the data of Fig. 12, at all three temperature values, the constant E can be evaluated from the slopes of the straight lines thus generated. [The plot is omitted for conciseness—see Ionescu (2006)]. Several data points at very low strain rates were disregarded due to the large uncertainty in measuring ΔT when this quantity is nearly zero; however, the remaining data generated nearly perfect, overlapping straight lines with an average E of $2.76 \pm .04 \times 10^{-7}$.

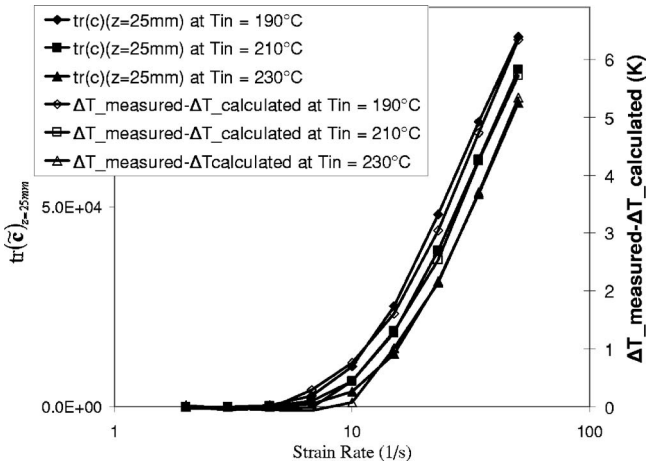

FIG. 12. Correlation between the degree of orientation developed in the die and the deviation of the measured temperature increase from the theoretical prediction.

C. Complete form of the temperature equation

Rewriting the complete form of the energy equation, (17), for an incompressible fluid at steady state, one obtains

$$\rho \hat{c}_v(\mathbf{v}\cdot\nabla T) + \rho \left.\frac{\partial \hat{U}}{\partial \mathbf{c}}\right|_T : (\mathbf{v}\cdot\nabla \mathbf{c}) = k\nabla^2 T + \tau : \nabla \mathbf{v}. \tag{62}$$

The focus of attention is now on the second term on the left side of Eq. (62). In Cartesian coordinates of uniaxial elongational flow, the term $(\mathbf{v}\cdot\nabla\mathbf{c})$ becomes

$$\mathbf{v}\cdot\nabla\mathbf{c} = \begin{pmatrix} v_z\dfrac{\partial c_{xx}}{\partial z} & 0 & 0 \\ 0 & v_z\dfrac{\partial c_{yy}}{\partial z} & 0 \\ 0 & 0 & v_z\dfrac{\partial c_{zz}}{\partial z} \end{pmatrix}. \tag{63}$$

For the same flow situation, the off-diagonal components of the conformation tensor are zero, and $(\partial\hat{U}/\partial\mathbf{c})$ is

$$\frac{\partial \hat{U}}{\partial \mathbf{c}} = \begin{pmatrix} \dfrac{\partial \hat{U}}{\partial c_{xx}} & 0 & 0 \\ 0 & \dfrac{\partial \hat{U}}{\partial c_{yy}} & 0 \\ 0 & 0 & \dfrac{\partial \hat{U}}{\partial c_{zz}} \end{pmatrix}. \tag{64}$$

Performing the double-dot product in the second term on the left side of Eq. (62), one obtains

$$\rho\frac{\partial \hat{U}}{\partial \mathbf{c}} : (\mathbf{v}\cdot\nabla\mathbf{c}) = \rho v_z\left(\frac{\partial \hat{U}}{\partial c_{xx}}\frac{\partial c_{xx}}{\partial z} + \frac{\partial \hat{U}}{\partial c_{yy}}\frac{\partial c_{yy}}{\partial z} + \frac{\partial \hat{U}}{\partial c_{zz}}\frac{\partial c_{zz}}{\partial z}\right). \tag{65}$$

Typically, the conformation tensor component in the direction of the flow, c_{zz}, is several orders of magnitude larger than the other two diagonal components in the high deformation regimes. Furthermore, the diagonal components of the conformation tensor normal to the direction of flow will asymptotically approach zero quite rapidly as a function of axial position; therefore, the first two terms inside the parentheses on the right side of Eq. (65) will be several orders of magnitude smaller than the third, and are neglected henceforth. The entirety of Eq. (65) is nearly zero at low deformation rates, so this act of negligence is considered as inconsequential over the entire range of deformations studied.

Combining Eqs. (62) and (65), an appropriate form of the temperature evolution equation is derived as

$$\rho\hat{c}_v(\mathbf{v}\cdot\nabla T) = k\nabla^2 T + \left[\tau : \nabla\mathbf{v} - \rho v_z\left(\frac{\partial \hat{U}}{\partial c_{zz}}\frac{\partial c_{zz}}{\partial z}\right)\right]. \tag{66}$$

Comparing this equation to its traditional form as derived using the PEE assumption, Eq. (29), one notices the appearance of an extra heat generation term inside the square

brackets on the right side. Normally, the minus sign in front of that term would indicate a heat loss; however, atomistic simulations indicate that the internal energy of the melt decreases with increasing degree of orientation [Ionescu *et al.* (2007); Mavrantzas and Theodorou (1998); Mavrantzas and Öttinger (2002)]. Therefore, the derivative $\partial\hat{U}/\partial c_{zz}$ is always negative, making the extra term a source of heat, rather than a sink. Indeed, the experiments indicated that the traditional temperature equation, (29), under-predicted the measured temperature profiles; therefore, it is highly likely that this extra heat generation will provide an improvement over the previous FE simulations.

Using Eq. (66), two corrections are thus made to the traditional temperature equation. The first correction involves introducing the conformation tensor functionality into the heat capacity according to Eq. (18). In the following, this amendment is referred to as "correction 1." The second correction involves introducing the conformational dependence of the internal energy into the total heat generation term. This is referred to as "correction 2." The relative importance of these two corrections can then be discussed.

Using the FE procedure described in Sec. III D, the new temperature equation, (66), is introduced and solved under the same conditions as above. Having the functional forms of the conformation tensor components with respect to axial position completely defined [Eqs. (57) and (58)], it is simple to evaluate the conformational contribution to the heat capacity, Eq. (18), and the axial gradient of $c_{zz}(\partial c_{zz}/\partial z)$. The only missing piece of information is $\partial\hat{U}/\partial c_{zz}$. Using the UCMM, Dressler *et al.* (1999) and Dressler (2000) derived the functional form for the internal energy density of a fluid element as

$$u = \frac{1}{2}\rho\gamma\left(K(T) - T\frac{\partial K(T)}{\partial T}\right)\mathrm{tr}(\mathbf{c}), \tag{67}$$

where u is the internal energy density of the element. At high degrees of orientation, the diagonal component of the conformation tensor in the direction of the deformation, c_{zz}, is several orders of magnitude larger than the other two, which makes it identifiable with the trace of the conformation tensor. Consequently, the derivative of the internal energy with respect to c_{zz} is approximately equal to the derivative with respect to $\mathrm{tr}(\mathbf{c})$. Mathematically, this approximation can be expressed as

$$c_{zz} \approx \mathrm{tr}(\mathbf{c}) \Rightarrow \frac{\partial\hat{U}}{\partial c_{zz}} \approx \frac{\partial\hat{U}}{\partial\mathrm{tr}(\mathbf{c})}. \tag{68}$$

Combining Eqs. (67) and (68) and transforming to proper dimensions, one derives the derivative of the internal energy with respect to c_{zz} from Eq. (66) as

$$\frac{\partial\hat{U}}{\partial c_{zz}} = \frac{1}{2}\gamma\left(K(T) - T\frac{\partial K(T)}{\partial T}\right). \tag{69}$$

Combining Eqs. (19), (20), and (69) subsequently yields

$$\frac{\partial\hat{U}}{\partial c_{zz}} = \frac{1}{2}\gamma k_B T(B+1). \tag{70}$$

In the subsequent analysis, the value for B was taken as the experimental value of Ciferri *et al.* (1961) for a polyethylene melt, $B=-1.45$ (see Sec. II C for details). Equations (67)–(70) also apply to the Giesekus model, since it shares the same free energy expression with the UCMM [Booij (1984); Beris and Edwards (1994)]. However, in the case of the Giesekus model, the components of the conformation tensor and their derivatives with respect to axial position are different than the UCMM, as given by Eq. (59).

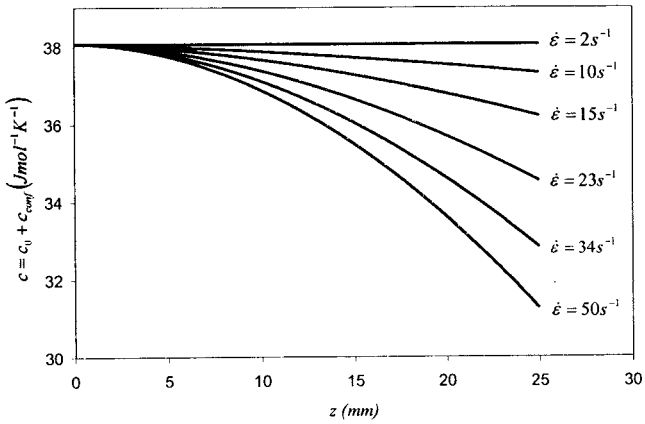

FIG. 13. The total heat capacity predicted by UCMM for the HDPE melt at T_{in}=190 °C.

With the extra generation term of Eq. (66) completely defined, a new set of FE calculations was performed to determine the relative magnitude of corrections 1 and 2 mentioned above.

First, it is very interesting to examine the total heat capacity [Eq. (18)] as a function of axial position for the HDPE melt at T_{in}=190 °C. In Fig. 13, the total heat capacity assuming the UCMM conformation tensor is shown for selected strain rates. One observes a reduction in the heat capacity of up to 18% at the die exit for the highest value the strain rate. This axial position functionality is then embedded into the FE methodology. This accounts for correction 1, as defined above.

The extra heat generation term was inserted into the FE program, as expressed by Eqs. (58) and (70) for the UCMM. In the case of the Giesekus model, the derivative of the internal energy with respect to c_{zz} is also stated in Eq. (70), while the numerical solution to Eq. (59) was used to obtain the derivative of c_{zz} with respect to axial position.

Figure 14 presents the temperature changes due to elongational deformation calculated using the traditional temperature equation, (29), the experimental temperature changes, and the calculated temperature profiles by adding corrections 1 and 2 to the traditional temperature equation for the HDPE melt at T_{in}=190 °C. Even though the predicted heat capacity changes were quite significant (see Fig. 13), correcting for the conformational part of the heat capacity yields results that are virtually indistinguishable from the ones calculated using the traditional temperature equation; however there is a very slight increase of ΔT over the uncorrected temperature equation. The physical cause of this behavior is again attributed to the competition between different phenomena. First, as the heat capacity decreases with the degree of orientation, the fluid is able to retain less heat, and the temperature rises more quickly than under no applied deformation. From this phenomenon acting alone, one would expect a larger ΔT than for a constant heat capacity. However, as the temperature rises, the viscosity decreases, thus providing a reduction in the degree of heat generation. Furthermore, the amount of heat conducted out of the fluid increases as the temperature increases, due to a larger temperature gradient driving force toward the wall. In short, the only significant changes in the heat capacity occur just before the die exit (see Fig. 13), leaving little opportunity for any substantial deviations from constant heat capacity behavior.

The inclusion of the extra generation term in the temperature equation yields a significant quantitative improvement over the previous simulation results, and this corre-

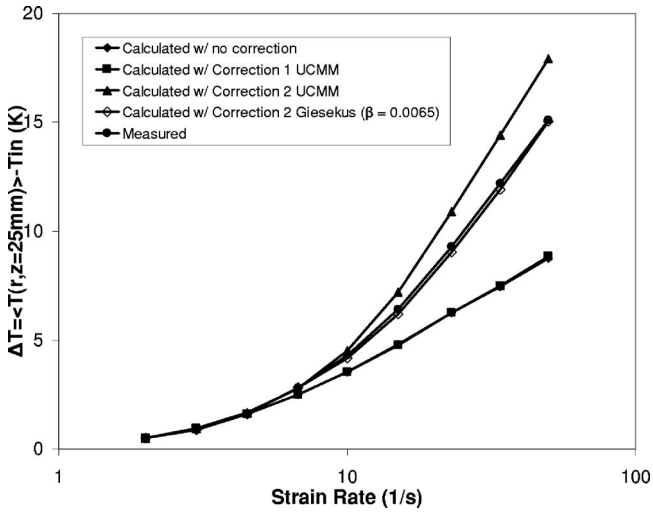

FIG. 14. Relative effects of correcting for the conformational part of the heat capacity (correction 1) and for the extra heat generation term (correction 2) in the calculated temperature profiles for the HDPE melt at T_{in} = 190 °C.

sponds to improved quantitative agreement with the experimental values. However, as seen from Fig. 14, adding correction 2 from the UCMM yields a slight over-prediction of the measured values. Nevertheless, it is clearly evident that correction 2 can indeed account for the large discrepancy between the experimental and simulated temperature rises.

It is probably too much to expect that the UCMM would match perfectly the experimental data, given that it cannot describe the nonlinear rheological characteristics of polymer melts. Therefore, the Giesekus model was also examined, since it is widely considered to be a reasonably good example of a simple viscoelastic model that describes well the most important rheological and microstructural properties [Baig *et al.* (2006)]. Using this model, an iterative procedure was used to match the measured temperature profiles by varying β as a fitting parameter. The value of β that yielded the best match was β=0.0065. It is worth emphasizing that for β=0, the UCMM is recovered. Note that a plot of $\mathrm{tr}\tilde{\mathbf{c}}$ vs. Giesekus parameter (not shown) at the die exit shows that $\mathrm{tr}\tilde{\mathbf{c}}$ increases very rapidly to a plateau value with increasing β. In fact, by β=0.05, this plateau is attained. By extending the value of this parameter up to 0.4, there is practically no change in $\mathrm{tr}\tilde{\mathbf{c}}$ from 0.05 to 0.4. At 0.4, the prediction of the model is only one degree less at the highest strain rate than was the case for β=0.0065. However, this value of β value does give the best fit, since for β<0.05, $\mathrm{tr}\tilde{\mathbf{c}}$ changes dramatically. The value obtained from the simulations of 0.0065 is not far from zero, which implies that the necessary correction to the UCMM was minimal. It thus seems reasonable to assume that the extra heat generation term is necessary for describing accurately the experimental behavior at high deformation rates. Hence the primary assumption of PEE must be seriously reconsidered under such conditions.

V. CONCLUDING REMARKS

The underlying theme of this study was to investigate the nature of the elastic energy stored by polymer melts when subjected to deformation using experimental measure-

ments, macroscopic theory, and simulation. Contrary to common views, the model polymer (polyethylene) was shown to exhibit strong energetic effects when subjected to uniaxial elongational stretching.

In Sec. III, it was established that the assumption of PEE is not universally valid, as often assumed. Experimental evidence showed that the assumption of PEE is not valid for polymers at high strain rates. These statements above have two major consequences with far reaching implications. First, the classical temperature evolution equation used in nearly every engineering analysis of nonisothermal polymer flows to date only seems to be valid for low to intermediate deformation rates. For wider ranges of deformation, when significant orientation is present, a more general form of the temperature evolution equation is needed, which contains additional terms accounting for internal structural contributions to the internal energy. However, as shown in Sec. II C, under appropriate flow conditions, these terms can vanish. In the case of elongational flow generated inside the Hencky dies investigated in this study, the fluid is not homogeneous in terms of internal orientation ($\nabla \mathbf{c} \neq 0$); thus the second term on the left side of Eq. (17) is nonzero. As demonstrated in Sec. IV, the extra term accounting for internal orientation is significant, and it should therefore be included in a complete analysis. Second, the constant volume heat capacity ceases to be a constant with respect to deformation rate at high degrees of orientation. This behavior needs to be incorporated into the temperature evolution equation as well, although it was shown that incorporating the structural information into the heat capacity has a negligible effect on the predicted temperature profiles. However, this statement might not hold true in general.

The work presented in this study has clarified some important aspects concerning the nonisothermal flow of polymer melts. Given the large number of industrial applications involving nonisothermal flows under high deformation rates, it is possible that the present study might open a path forward for more research in this somewhat neglected area.

ACKNOWLEDGMENTS

This research was supported by the donors of the Petroleum Research Fund, administered under Grant No. 41000-AC7. This research project also used resources of the Center for Computational Sciences at Oak Ridge National Laboratory, which is supported by the Office of Science, U. S. Department of Energy, under Contract No. DE-AC05-00OR22725, managed and operated by UT-Battelle, LLC.

References

Astarita, G., "Thermodynamics of dissipative materials with entropic elasticity," Polym. Eng. Sci. **14**, 730–733 (1974).

Astarita, G., and G. C. Sarti, "The dissipative mechanism in flowing polymers: Theory and experiments," J. Non-Newtonian Fluid Mech. **1**, 39–50 (1976a).

Astarita, G., and G. C. Sarti, "An approach to thermodynamics of polymer flow based on internal state variables," Polym. Eng. Sci. **16**, 490–495 (1976b).

Baig, C., B. Jiang, B. J. Edwards, D. J. Keffer, and H. D. Cochran, "A comparison of simple rheological models and simulation data of n-hexadecane under shear and elongational flow," J. Rheol. **50**, 625–640 (2006).

Balasubramanian, V., K. Bush, S. Smoukov, D. C. Venerus, and J. D. Schieber, "Measurements of flow-induced anisotropic thermal conduction in a polyisobutylene melt following step shear flow," Macromolecules **38**, 6210–6215 (2005).

Bedrov, D., and G. D. Smith, "The role of local conformations in the stretching of a poly(ethylene oxide) chain

in solution," J. Chem. Phys. **118**, 6656–6663 (2003).
Beris, A. N., and B. J. Edwards, "Poisson bracket formulation of incompressible flow equations in continuum mechanics," J. Rheol. **34**, 55–78 (1990a).
Beris, A. N., and B. J. Edwards, "Poisson bracket formulation of viscoelastic flow equations of differential type: A unified approach," J. Rheol. **34**, 503–538 (1990b).
Beris, A. N., and B. J. Edwards, *Thermodynamics of Flowing Systems* (Oxford University Press, Oxford, UK, 1994).
Bird, R. B., "Use of simple molecular models in the study of the mechanical behaviour of solution of flexible macromolecules," J. Non-Newtonian Fluid Mech. **5**, 1–12 (1979).
Bird, R. B., R. C. Armstrong, and O. Hassager, *Dynamics of Polymeric Liquids*, 2nd ed. (Wiley, New York, 1987), Vol. 1.
Bird, R. B., W. E. Stewart, and E. N. Lightfoot, *Transport Phenomena*, 2nd ed. (Wiley, New York, 2002).
Booij, H. C., "The energy storage in the Rouse model in an arbitrary flow field," J. Chem. Phys. **80**, 4571–4572 (1984).
Brandrup, J., E. H. Immergut, E. A. Grulke, A. Abe, and D. R. Bloch, eds., *Polymer Handbook*, 4th ed. (Wiley-Interscience, New York, 1999).
Choy, C. L., W. H. Luk, and F. C. Chen, "Thermal conductivity of highly oriented polyethylene," Polymer **19**, 155–162 (1978).
Choy, C. L., Y. Fei, and T. G. Xi, "Thermal conductivity of gel-spun polyethylene fibers," J. Polym. Sci., Part B: Polym. Phys. **31**, 365–370 (1993).
Ciferri, A., C. A. J. Hoeve, and P. J. Flory, "Stress-temperature coefficients of polymer networks and conformational energy of polymer chains," J. Am. Chem. Soc. **83**, 1015–1022 (1961).
Collier, J. R., US Patent No. 5,357,784 (1994).
Collier, J. R., O. Romanoschi, and S. Petrovan, "Elongational rheology of polymer melts and solutions," J. Appl. Polym. Sci. **69**, 2357–2367 (1998).
Dai, S. C., and R. I. Tanner, "Anisotropic thermal conductivity in sheared polypropylene," Rheol. Acta **45**, 228–238 (2006).
Dressler, M., (2000). "The dynamical theory of non-isothermal polymeric materials," Ph.D. Dissertation, ETH, Zurich (2000).
Dressler, M., B. J. Edwards, and H. C. Ottinger, "Macroscopic thermodynamics of flowing polymeric liquids," Rheol. Acta **38**, 117–136 (1999).
Edwards, B. J., and A. N. Beris, "Non-canonical Poisson bracket for nonlinear elasticity with extension to viscoelasticity," J. Phys. A **24**, 2461–2480 (1991a).
Edwards, B. J., and A. N. Beris, "Unified view of transport phenomena based on the generalized bracket formulation," Ind. Eng. Chem. Res. **30**, 873–881 (1991b).
Edwards, B. J., S. Petrovan, J. R. Collier, K. Feigl, and F. X. Tanner, "Simulating and measuring elongational flow properties in special geometries," *7th World Congress of Chemical Engineering*, [CD-ROM], Glasgow, Scotland, July 10–14 (2005).
Feigl, K., F. Tanner, B. J. Edwards, and J. R. Collier, "A numerical study of the measurement of elongational viscosity of polymeric fluids in a semihyperbolically converging die," J. Non-Newtonian Fluid Mech. **115**, 191–215 (2003).
Gaur, U., and B. Wunderlich, "Heat capacity and other thermodynamic properties of linear macromolecules. II. Polyethylene," J. Phys. Chem. Ref. Data **110**, 119–152 (1981).
Giesekus, H., "A simple constitutive equation for polymer fluids based on the concept of deformation-dependent tensorial mobility," J. Non-Newtonian Fluid Mech. **11**, 69–109 (1982).
Gupta, R. K., and A. B. Metzner, "Modeling of non-isothermal polymer processes," J. Rheol. **26**, 181–198 (1982).
Hands, D., "The effect of biaxial orientation on the thermal conductivity of vulcanized and unvulcanized rubber," Rubber Chem. Technol. **53**, 80–87 (1980).
Hansen, D., and C. C. Ho, "Thermal conductivity of high polymers," J. Polym. Sci. A **3**, 659–670 (1965).
Iddir, H., D. C. Venerus, and J. D. Schieber, "Measuring anisotropic thermal conduction in polyisobutylene following step shear strains," AIChE J. **46**, 610–615 (2000).

Ionescu, T., "Thermodynamic characterization of polymeric materials subjected to non-isothermal flows: Experiment, theory and simulation," Ph.D. dissertation, The University of Tennessee (2006).

Ionescu, T. C., C. Baig, B. J. Edwards, D. J. Keffer, and A. Habenschuss, "Structure formation under steady-state isothermal planar elongational flow of n-eicosane: A comparison between simulation and experiment," Phys. Rev. Lett. **96**, 037802; 1–4 (2006).

Ionescu, T. C., V. G. Mavrantzas, D. J. Keffer, and B. J. Edwards, J. Rheol., submitted (2007).

Kamerkar, P. A., and B. J. Edwards, "An experimental study of slip flow in capillary and semi-hyperbolically converging dies," Polym. Eng. Sci. **47**, 159–167 (2006).

Kurabayashi, K., "Anisotropic thermal properties of solid polymers," Int. J. Thermophys. **22**, 277–288 (2001).

Lu, Z. Y., W. Nowak, G. R. Lee, P. E. Marszalek, and W. T. Yang, "Elastic properties of single amylose chains in water: A quantum mechanical and AFM study," J. Am. Chem. Soc. **126**, 9033–9041 (2004).

Marrucci, G., "The free energy constitutive equation for polymer solution from the dumbbell model," Trans. Soc. Rheol. **16**, 321–330 (1972).

Mavrantzas, V. G., and D. N. Theodorou, "Atomistic simulation of polymer melt elasticity: Calculation of the free energy of an oriented polymer melt," Macromolecules **31**, 6310–6332 (1998).

Mavrantzas, V. G., and H. C. Ottinger, "Atomistic Monte Carlo simulations of polymer melt elasticity: Their nonequilibrium thermodynamics GENERIC formulation in a generalized canonical ensemble," Macromolecules **35**, 960–975 (2002).

Meissner, J., "Development of a universal extensional rheometer for uniaxial extension of polymer melts," Trans. Soc. Rheol. **16**, 405–420 (1972).

Meissner, J., "Experimental aspects in polymer melt elongational rheometry," Chem. Eng. Commun. **33**, 159–180 (1985).

Meissner, J., and J. Hostettler, "A new elongational rheometer for polymer melts and other highly viscoelastic liquids," Rheol. Acta **33**, 1–21 (1994).

Nakajima, K., H. Watabe, and T. Nishi, "Single polymer chain rubber elasticity investigated by atomic force microscopy," Polymer **47**, 2505–2510 (2006).

Oldroyd, J. G., "On the formulation of rheological equations of state," Proc. R. Soc. London, Ser. A **200**, 523–541 (1950).

Ortiz, C., and G. Hadziioannou, "Entropic elasticity of single polymer chains of poly(methacrylic acid) measured by atomic force microscopy," Macromolecules **32**, 780–787 (1999).

Petrovan, S., J. R. Collier, and G. H. Morton, "Rheology of cellulosic n-methylmorpholine oxide monohydrate solutions," J. Appl. Polym. Sci. **77**, 1369–1377 (2000).

Sarti, G. C., and N. Esposito, "Testing thermodynamic constitutive equations for polymers by adiabatic deformation experiments," J. Non-Newtonian Fluid Mech. **3**, 65–76 (1977).

Shi, W. Q., Y. H. Zhang, C. J. Liu, Z. Q. Wang, X. Zhang, and Y. M. Chen, "Toward understanding the effect of substitutes and solvents on entropic and enthalpic elasticity of single dendronized copolymers," Polymer **47**, 2499–2504 (2006).

Smith, J. S., D. Bedrov, G. D. Smith, and E. M. Kober, "Thermodynamic and conformational changes upon stretching a poly(dimethylsiloxane) chain in the melt," Macromolecules **38**, 8101–8107 (2005).

Treloar, L. R. G., *The Physics of Rubber Elasticity* (Clarendon Press, Oxford, UK, 1975).

van den Brule, B., "A network theory for the thermal conductivity of an amorphous polymeric material," Rheol. Acta **28**, 257–266 (1989).

Venerus, D. C., private communication (2006).

Venerus, D. C., J. D. Schieber, H. Iddir, J. D. Guzman, and A. W. Broerman, "Measurement of thermal diffusivity in polymer melts using forced Rayleigh light scattering," J. Polym. Sci., Part B: Polym. Phys. **37**, 1069–1078 (1999a).

Venerus, D. C., J. D. Schieber, H. Iddir, J. D. Guzman, and A. W. Broerman, "Relaxation of anisotropic thermal diffusivity in a polymer melt following step shear strain," Phys. Rev. Lett. **82**, 366–369 (1999b).

Venerus, D. C., J. D. Schieber, H. Iddir, J. Guzman, and A. Broerman, "Anisotropic thermal diffusivity measurements in deforming polymers and the stress-thermal rule," Int. J. Thermophys. **22**, 1215–1225 (2001).

Venerus, D. C., J. D. Schieber, V. Balasubramanian, K. Bush, and S. Smoukov, "Anisotropic thermal conduction in a polymer liquid subjected to shear flow," Phys. Rev. Lett. **93**, 098301 (2004).

Wallace, D. J., C. Moreland, and J. J. C. Picot, "Shear dependence of thermal conductivity in polyethylene melts," Polym. Eng. Sci. **25**, 70–74 (1985).

Wapperom, P., and M. A. Hulsen, "Thermodynamics of viscoelastic fluids: The temperature equation," J. Rheol. **42**, 999–1019 (1998).

Wiest, J. M., "Time-temperature superposition in nonisothermal flow," J. Non-Newtonian Fluid Mech. **27**, 127–131 (1988).